Am J Cancer Res 2022;12(11):4954-4976
www.ajcr.us /ISSN:2156-6976/ajcr0145790

Original Article

Multi-omics analysis of kinesin family member 2C in human tumors: novel prognostic biomarker and tumor microenvironment regulator

Bixi Zhang[1*], Peng Liu[2*], Yanchun Li[1], Qing Hu[1], Huan Li[2], Xiaoyang Pang[3], Hao Wu[2,4]

[1]Department of Pathology, Hunan Provincial People's Hospital, Hunan Normal University, Changsha, Hunan, China; [2]Department of Gastroenterology, Third Xiangya Hospital, Central South University, Changsha, Hunan, China; [3]Department of Orthopaedics, Xiangya Hospital, Central South University, Changsha, Hunan, China; [4]Center for Precision Medicine, University of Missouri School of Medicine, Columbia, MO, USA. [*]Equal contributors.

Received August 7, 2022; Accepted October 26, 2022; Epub November 15, 2022; Published November 30, 2022

Abstract: Kinesin family member 2C (KIF2C) is the best-characterized member of the kinesin-13 family and is involved in accurately fine-tuned dynamics of mitotic spindles. As KIF2C is involved in both spindle formation and regulation of DNA double-strand breaks, precise regulation of KIF2C is essential to prevent malignant transformation associated with gains and losses of DNA content. In the present study, we initially reviewed The Cancer Genome Atlas database and observed that KIF2C is abundantly expressed in most tumor types. We then analyzed the gene alteration profile, protein expression, prognosis, and immune reactivities of KIF2C in more than 10,000 samples from several well-established databases. In addition, we conducted a gene enrichment set analysis to investigate the potential mechanisms underlying the role of KIF2C in tumorigenesis. Multi-omics analysis of KIF2C demonstrated significant statistical correlations between KIF2C expression and clinical prognosis, oncogenic signature gene sets, myeloid-derived suppressor cell infiltration, ImmunoScore, immune checkpoints, microsatellite instability, and tumor mutational burden across multiple tumors. Single-cell data showed that KIF2C is abundantly expressed in malignant cells. The experimental validation demonstrated that KIF2C is highly expressed in gastric cancer cell lines, gastric adenocarcinoma, and hepatocelluar carcinoma. The findings of this study provide important insight for understanding the role and mechanisms of KIF2C in tumorigenesis and immunotherapy in a variety of cancers.

Keywords: KIF2C, pan-cancer, MDSCs, immunotherapy, prognosis

Introduction

A preprint has previously been published [1]. Kinesin family member 2C (KIF2C), also known as mitotic centromere-associated kinesin (MCAK), is the best-characterized member of the kinesin-13 family and is involved in accurately fine-tuned dynamics of mitotic spindles [2]. KIF2C is predominantly found in centrosomes, centromeres, and microtubules [3, 4]. Chromosomal instability, a hallmark of tumor cells, can be induced by defective DNA repair due to erroneous chromosome segregation during mitosis [5]. As KIF2C is involved in both spindle formation and regulation of DNA double-strand breaks, precise regulation of KIF2C is essential to prevent malignant transformation associated with gains and losses of DNA content [6]. Hyperactive kinases (e.g., aurora kinase A and polo-like kinase 1) or inactive p53 could deregulate KIF2C to the extent that chromosomal instability and aneuploidy are promoted [7].

Accumulating evidence has demonstrated that KIF2C is aberrantly regulated during malignancy. KIF2C is highly expressed in hepatocellular carcinoma and colorectal cancer and is associated with a poor prognosis [8, 9]. However, the mechanisms underlying the role of KIF2C in tumorigenesis in various cancers have not been well defined. We reviewed The Cancer Genome Atlas (TCGA) database and found that *KIF2C* is abundantly expressed in most cancers of diverse origins. Thus, pan-cancer analysis of

KIF2C may provide new insights into the molecular mechanisms underlying tumor occurrence, recurrence, and immunotherapy.

In the present study, we analyzed the profiles of gene alterations, protein expression, prognosis, and immune reactivities of KIF2C in more than 10,000 samples from several well-established datasets. We also conducted a *KIF2C*-related gene enrichment analysis to investigate the potential mechanisms underlying the role of *KIF2C* in tumorigenesis. In addition, the expression of KIF2C have been validated in human gastric cancer cell lines and patients tumor samples. This study aimed to examine the roles and potential mechanisms of KIF2C in the development and progression of human cancers.

Materials and methods

Genetic alteration analysis

The genetic alteration characteristics of *KIF2C* were queried from "TCGA PanCancer Atlas Studies" module of cBioPortal (https://www.cbioportal.org/, accessed on January 15, 2022) [10]. The details of the tumor entity summary, alteration frequency, and copy number alteration (CNA) are shown in the "Cancer Types Summary" module. The diagram of *KIF2C* alteration sites that included the alteration types, case number, and 3D molecular structure were obtained from the "mutations" module.

Gene expression analysis

Considering adjacent normal tissue as a control or even no control group in tumors from TCGA database, Genotype-Tissue Expression (GTEx) database was obtained for corresponding normal tissues as the control group. The difference of *KIF2C* expression between certain tumor tissues and normal tissues was carried out through the "Box Plot" module of Gene Expression Profiling Interactive Analysis, version 2 (GEPIA2) (http://gepia2.cancer-pku.cn/, accessed on January 15, 2022) [11]. Additionally, we obtained plots of the KIF2C expression in different pathological stages of TCGA tumors via the "Pathological Stage Plot" module of GEPIA2. We further obtained plots of the KIF2C expression in different cancer cell lines via Cancer Cell Line Encyclopedia (CCLE) (https://depmap.org/portal/gene/, accessed on January 16, 2022) [12]. UALCAN (http://ualcan.path.uab.edu/analysis-prot.html, accessed on January 17, 2022) [13] was used to conduct KIF2C protein expression analysis in the Clinical Proteomic Tumor Analysis Consortium (CPTAC) Confirmatory/Discovery database. The Human Protein Atlas (HPA) database (https://www.proteinatlas.org/, accessed on January 17, 2022) was used to obtain the RNA expression level of *KIF2C* in normal tissues and immunohistochemical staining images of KIF2C expression in human tumors and normal tissues.

Survival analysis

The Kaplan-Meier survival map module of GEPIA2 was used to obtain the overall survival (OS) and disease-free survival (DFS) heatmap data of KIF2C across all cancers in TCGA cohort. The log-rank test was applied in the hypothesis test, and survival plots were obtained through the Kaplan-Meier "Survival Analysis" module of GEPIA2.

The protein-protein interaction of KIF2C and similar genes in pan-cancer

Using STRING (https://string-db.org/, accessed on January 18, 2022) tool, protein-protein interaction (PPI) analysis of KIF2C will present 50 available experimentally determined KIF2C-interacted proteins and visualize the PPI network. Moreover, based on cancer data from TCGA cohort, the top 100 *KIF2C*-correlated targeting genes were obtained from the "Similar Genes Detection" module of GEPIA2. Utilizing the "correlation analysis" module of GEPIA2, a pairwise gene Pearson's correlation analysis of *KIF2C* and the top five selected genes was performed. Spearman's correlation test was performed on the top five selected genes using the "Gene_Corr" module of TIMER2 to obtain a heatmap.

Using Venn Diagram (http://bioinformatics.psb.ugent.be/webtools/Venn/, accessed on January 19, 2022), we conducted an intersection analysis to compare the KIF2C-interacted and KIF2C-correlated genes. In addition, combining the two sets of data, R package "clusterProfiler" in R software (Version 4.1.1, R Foundation for Statistical Computing, Vienna, Austria) was used to perform Kyoto Encyclopedia of Genes and Genomes (KEGG) pathway and Gene

Ontology (GO) enrichment analysis including biological process, molecular function, and cellular component.

Gene set enrichment analysis of KIF2C in pan-cancer

To explore the biological and oncogenic signaling pathways, Gene Set Enrichment Analysis (GSEA) was performed in high-and low-expression groups based on the mean expression value of *KIF2C* in 33 cancers of TCGA dataset. R package "clusterProfiler" in R software was used to perform MSigDB H (hallmark gene sets) and C6 (oncogenic signature gene sets) enrichment analysis. Gene sets with |NES|>1, p. adjust <0.05, and FDR<0.25 were considered significantly enriched.

Immune infiltration analysis

To explore the association between *KIF2C* expression and immune infiltration of all cancers in TCGA database, we input *KIF2C* in "gene expression" module, while myeloid derived suppressor cells (MDSCs) in "immune infiltrates" module of TIMER2 to obtain a heatmap and the scatter plots.

The Sangerbox platform (http://sangerbox.com/, accessed on January 20, 2022) was used to generate the Stromal, Immune, and ESTIMATE scores. In addition, the relationship between KIF2C expression and various immune checkpoints (inhibitory and stimulatory) was explored. The correlation between *KIF2C* expression and tumor mutational burden (TMB) and microsatellite instability (MSI) in different cancers in TCGA database was also analyzed using Sangerbox. Cellular heterogeneity of KIF2C expression in various cancers was conducted using Cancer Single-cell Expression Map (https://ngdc.cncb.ac.cn/cancerscem/index, last accessed on March 1, 2022) [14].

Cell culture

GES-1, SGC-7901, HGC-27, MKN-45, and AGS are purchased from ATCC. All the cells were cultured in Roswell Park Memorial Institute 1640 (RPMI 1640, Gibco) supplemented with 10% FBS and 1% Penicillin-Streptomycin in a 37°C humidified incubator with a 5% CO_2 environment.

Quantitative RT-PCR

Total RNA was extracted with Trizol (15596026, Invitrogen) and cDNA was synthesized using the PrimeScript RT-PCR kit (RR055B, Takara) according to the manufacturer's instructions. A SYBR Green PCR Kit (4344463, Applied Biosystems) was used to conduct qRT-PCR on the CFX96 real-time PCR detection system. Relative KIF2C mRNA expression in cancer cells were measured by the $2^{-\Delta\Delta Ct}$ method. We normalized the expression levels to those of the internal control glyceraldehyde 3-phosphate dehydrogenase (GAPDH). Primer sequences are as follows: KIF2C (F: 5'-GGAGGAGAAGGCTATGGAAGA-3', R: 5'-TCGCAGGGCTGAGAAATG-3'); GAPDH (F: 5'-GGTCACCAGGGCTGCTTTA-3', R: 5'-GGATCTCGCTCCTGGAAGATG-3').

Western blot

Western blot the proteins through an SDS-PAGE gel and subsequently transferring them to 0.45 μm PVDF membrane (Merck). The membrane was blocked with 5% milk for 1 hour, and then incubated with the primary antibody (KIF2C: 28372-1-AP, Proteintech; GAPDH: 60004-1-Ig, Proteintech) overnight at 4°C. After three washes with TBST (each for 6 min), the membrane was incubated with the appropriate secondary antibodies at room temperature for 1 hour, washed with TBST, and visualized using the ECL by ChemoStudio Imaging System (Analytik Jena).

Immunohistochemical staining

The tumor tissue samples used in this study were obtained from patients who underwent surgical treatment and diagnosed with gastric cancer, liver hepatocellular, and lung adenocarcinoma at Hunan Provincial People's Hospital. All patients provided written informed consent. The present study was conducted in accordance with the Declaration of Helsinki, and all experiments were approved by the ethics committees of Hunan Provincial People's Hospital. Tissues were subjected to standard tissue processing and paraffin embedding. The tissues were sliced serially into sections 3 μm thick for hematoxylin and eosin (H&E) staining. For immunohistochemical staining (IHC), the tissue sections were preheated in Tris-EDTA buffer

(pH 9.0) and then maintain at a sub-boiling temperature for 20 minutes to retrieve the immunoreactivities of antigens. To block endogenous peroxidase activity, quench the tissue sections with 3.0% hydrogen peroxide at room temperature for 10 minutes. Antibody against KIF2C (1:200 dilution, 28372-1-AP; Proteintech, Wuhan, China) was used to incubate the tissue sections for 1 hour at room temperature. Sections were incubated with MaxVision HRP-Polymer anti-Rabbit IHC Kit (KIT-5030, MXB Biotechnologies, Foochow, China) for 30 minutes. The working solution of DAB (DAB-2032, MXB Biotechnologies, Foochow, China) was applied to the tissue sections for the chromogenic reaction. The tissue sections were examined using an upright microscope (BX53, Olympus, Japan).

Statistical analysis

Gene expression data from the TCGA and GTEx databases were analyzed using Wilcoxon test. Protein expression data from UALCAN dataset was analyzed using Student's *t*-test. The survival data from GEPIA2 database was analyzed using log-rank test. R package "clusterProfiler" in R software (Version 4.1.1, R Foundation for Statistical Computing, Vienna, Austria) was used to perform KEGG pathway, GO, MSigDB H and C6 enrichment analysis. The correlation analysis was evaluated in the TIMER2 database using purity-adjusted Spearman's rho. The correlation analysis of ImmunoScore, StromalScore, and ESTIMATEScore, immune checkpoints, MSI, and TMB using Pearson's correlation coefficient. The $P<0.05$ was considered as statistically significant.

Results

Genetic alteration of KIF2C in cancers

The following tumor entities from TCGA cohort were included in this study: ACC, BLCA, BRCA, COAD, CHOL, CESC, DLBC, ESCA, GBM, HNSC, KICH, KIRC, KIRP, LAML, LGG, LIHC, LUAD, LUSC, MESO, OV, PAAD, PCPG, PRAD, READ, SARC, SKCM, STAD, TGCT, THCA, THYM, UCEC, UCS, and UVM (abbreviations and acronyms are listed in Table S1). The *KIF2C* genetic alteration profile of cancers in TCGA cohort showed that 1.8% of enrolled patients had genetic alterations (predominantly missense mutations and amplifications), and the patients with UCEC had the highest frequency (6.99%) of *KIF2C* genetic alterations (**Figure 1A**). As shown in **Figure 1B**, missense mutations were the most common, followed by splice site mutations. The 3D molecular structures of the KIF2C and A500T missense mutation are shown in **Figure 1C**. Notably, all these somatic mutations were classified as variants of uncertain significance.

Gene expression analysis data

Based on the consensus databases of HPA and GTEx, the expression patterns of *KIF2C* in different normal tissues are shown in Figure S1. *KIF2C* is abundantly expressed in the testis, bone marrow, and lymphoid tissues with high RNA levels. Analysis of the expression profile of *KIF2C* in different tumor and normal tissues in the consensus datasets from TCGA and GTEx demonstrated that the expression level of KIF2C was significantly higher in tumor tissues than in normal tissues across different types of cancers, such as BLCA, BRCA, CESC, CHOL, COAD, DLBC, ESCA, GBM, HNSC, LIHC, LUAD, LUSC, OV, PAAD, READ, SARC, SKCM, STAD, THYM, UCEC, and UCS (**Figure 2A**). In addition, *KIF2C* expression was significantly related to the pathological stages of ACC, BRCA, KIRC, KIRP, LIHC, and LUAD (Figure S2). *KIF2C* was abundantly expressed in different cancer cell lines in the CCLE dataset (**Figure 2B**; Table S2). In the CPTAC dataset, the total KIF2C protein expression was higher in primary cancers than in normal tissues for BRCA, LUAD, HNSC, COAD, LIHC, PAAD, OV, UCEC, and KIRC (**Figure 3A**). Immunohistochemical staining images from the HPA dataset showed that positive KIF2C staining was present in COAD, LUAD, and CESC tissues, but not in normal tissues (**Figure 3B**).

Survival analysis data

Based on the levels of *KIF2C* expression in cancers, the correlation between *KIF2C* expression and cancer prognosis was explored in TCGA cohort. It was found that increased levels of *KIF2C* expression were significantly associated with poor OS in ACC [HR, 9.2; $P<0.0001$], KICH [HR, 8.2; $P=0.018$], KIRC [HR, 1.5; $P=0.0057$], KIRP [HR, 2.9; $P=0.001$], LGG [HR, 2.9; $P<0.0001$], LIHC [HR, 2.2; $P<0.0001$], LUAD [HR, 1.4; $P=0.016$], MESO [HR, 3.9; $P<0.0001$], PAAD [HR, 1.6; $P=0.02$], and SKCM [HR, 1.4; $P=0.01$] (**Figure 4A**). High expression of *KIF2C* was also significantly associated with poor DFS

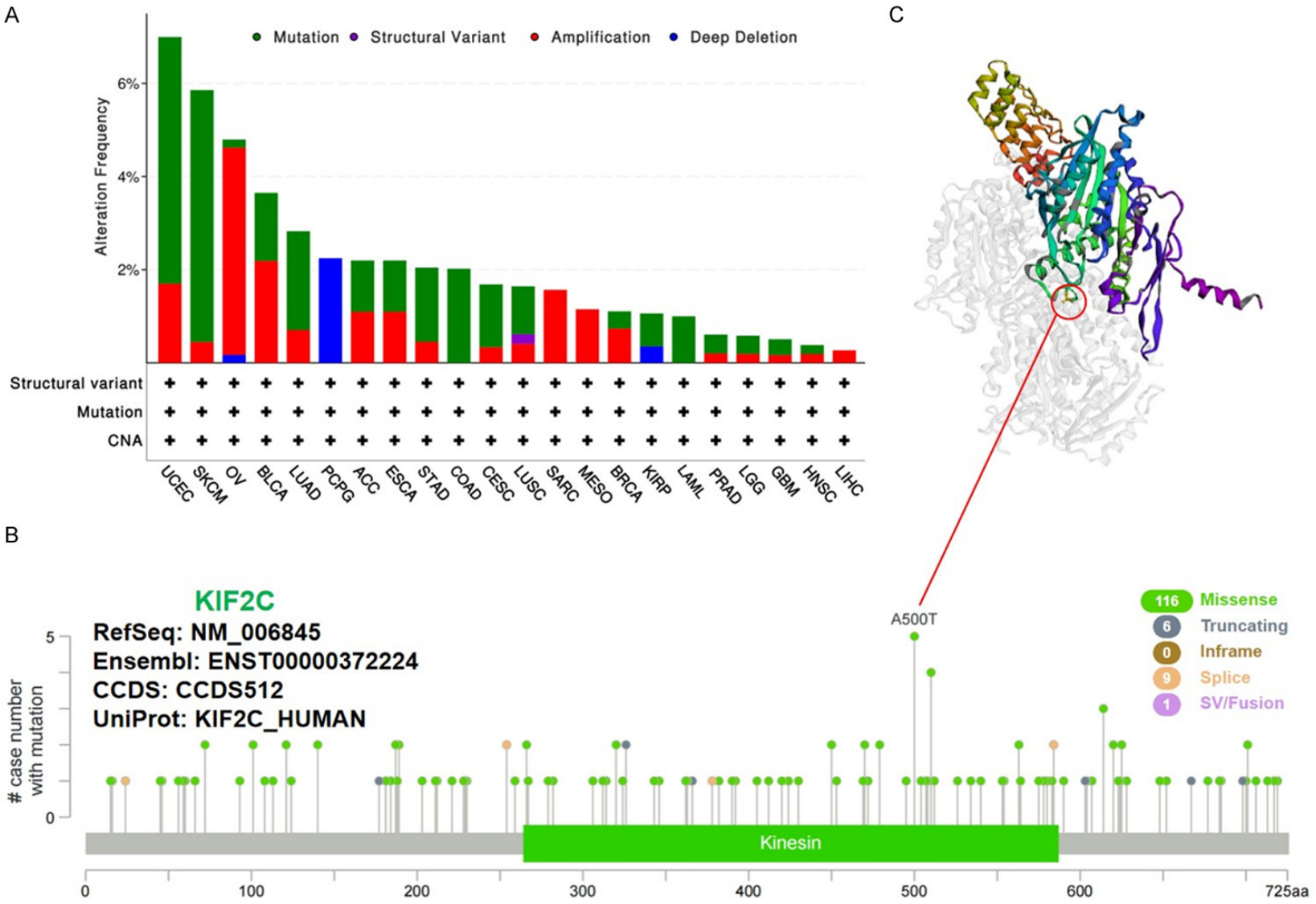

Figure 1. Genetic alterations of *KIF2C* in different tumors in TCGA database. A. Alteration frequencies with mutation types were displayed. B. The mutation site and case number of *KIF2C* genetic alterations were displayed. C. 3D molecular structure of KIF2C. CNA, copy number alteration; SV, structural variation.

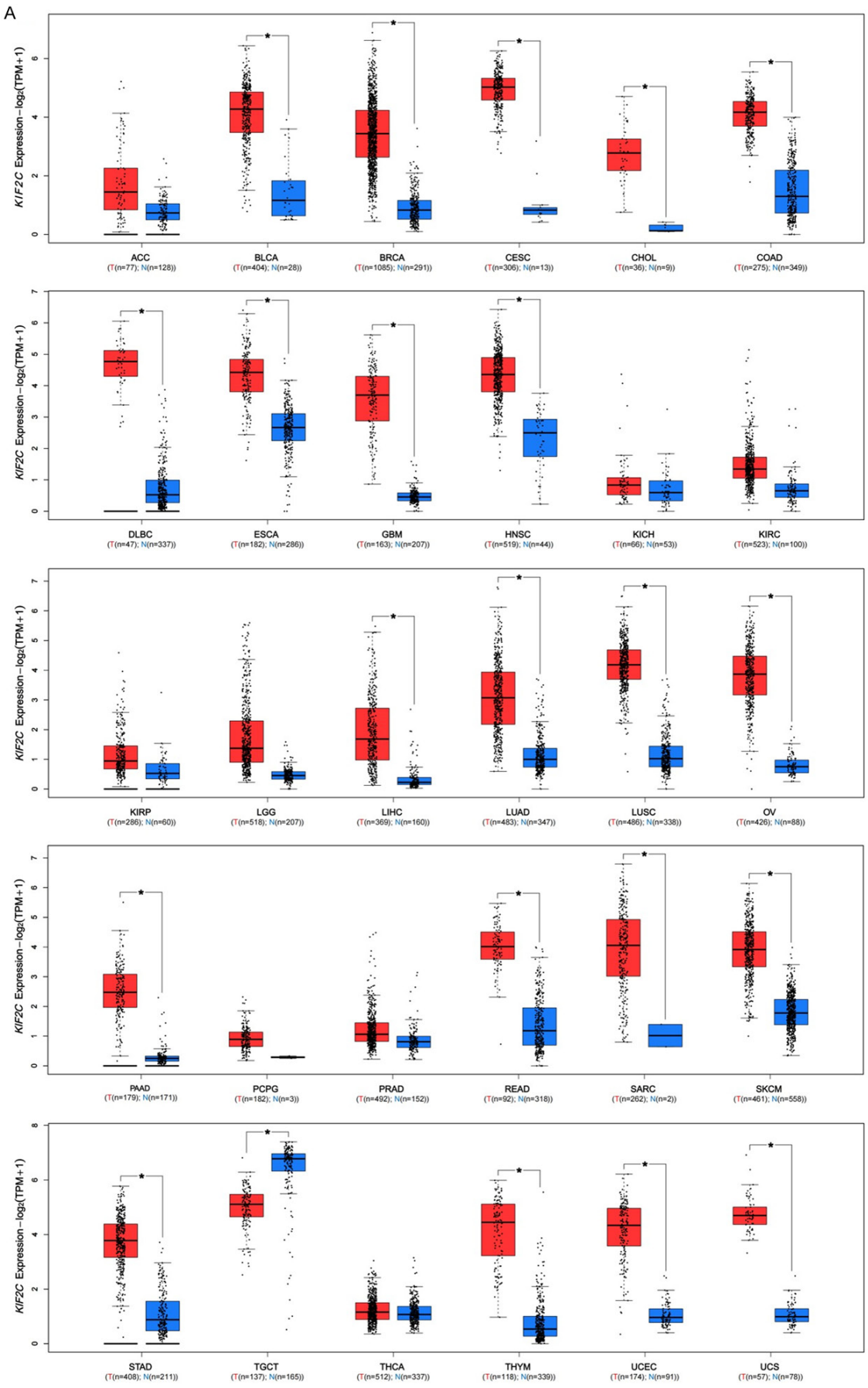
A
KIF2C Expression−log2(TPM+1)
ACC (T(n=77); N(n=128))
BLCA (T(n=404); N(n=28))
BRCA (T(n=1085); N(n=291))
CESC (T(n=306); N(n=13))
CHOL (T(n=36); N(n=9))
COAD (T(n=275); N(n=349))
DLBC (T(n=47); N(n=337))
ESCA (T(n=182); N(n=286))
GBM (T(n=163); N(n=207))
HNSC (T(n=519); N(n=44))
KICH (T(n=66); N(n=53))
KIRC (T(n=523); N(n=100))
KIRP (T(n=286); N(n=60))
LGG (T(n=518); N(n=207))
LIHC (T(n=369); N(n=160))
LUAD (T(n=483); N(n=347))
LUSC (T(n=486); N(n=338))
OV (T(n=426); N(n=88))
PAAD (T(n=179); N(n=171))
PCPG (T(n=182); N(n=3))
PRAD (T(n=492); N(n=152))
READ (T(n=92); N(n=318))
SARC (T(n=262); N(n=2))
SKCM (T(n=461); N(n=558))
STAD (T(n=408); N(n=211))
TGCT (T(n=137); N(n=165))
THCA (T(n=512); N(n=337))
THYM (T(n=118); N(n=339))
UCEC (T(n=174); N(n=91))
UCS (T(n=57); N(n=78))

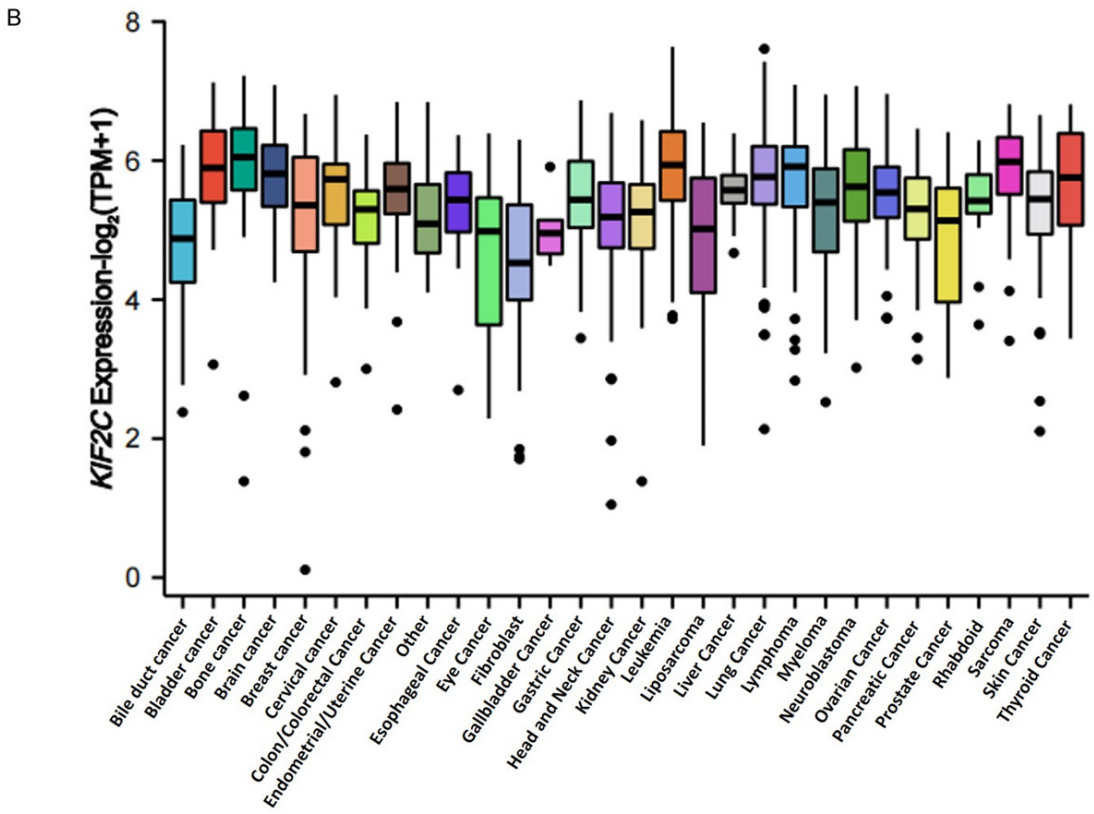

Figure 2. mRNA level expression of *KIF2C* in different tumors and cancer cell lines. A. The *KIF2C* expression level of different cancers in TCGA database compared with normal tissue in GTEx database. B. The *KIF2C* expression level of different cancer cell lines in the CCLE database. Log_2(TPM+1) transformed expression data for plotting. **P*<0.05, in Wilcoxon test. TPM, transcripts per million; N and T, normal and tumor tissue.

in ACC [HR, 5.2; *P*<0.0001], KIRC [HR, 1.8; *P*=0.0018], KIRP [HR, 3.8; *P*<0.0001], LGG [HR, 1.8; *P*=0.0001], LIHC [HR, 1.8; *P*<0.0001], MESO [HR, 2.1; *P*=0.016], PAAD [HR, 2.2; *P*=0.0005], PRAD [HR, 2.4; *P*=0.0001], and THCA [HR, 1.9; *P*=0.03] (**Figure 4B**).

Protein-protein interactions of KIF2C and similar genes in pan-cancer

To further investigate the potential mechanism of *KIF2C* in tumorigenesis, we conducted a series of enrichment analyses for proteins interacting with KIF2C and genes correlated with *KIF2C* based on STRING and GEPIA2. A total of 50 proteins that experimentally interacted with KIF2C are shown in the PPI network (**Figure 5A**). In addition, the top 100 *KIF2C*-correlated genes (Table S3) were identified, among which the top five genes were kinesin family member C1 (*KIFC1*) (R=0.85), cell division cycle 20 (*CDC20*) (R=0.84), non-SMC condensin I complex subunit H (*NCAPH*) (R=0.84), kinesin family member 4A (*KIF4A*) (R=0.83), and DLG-associated protein 5 (*DLGAP5*) (R=0.83) (**Figure 5B**). The corresponding heatmap data showed a significant and positive correlation between *KIF2C* and the top five genes in all cancer types in TCGA cohort (**Figure 5C**). Intersection analysis of the genes directly interacting with or related to KIF2C identified six genes, namely, aurora kinase A (*AURKA*), kinesin family member 14 (*KIF14*), kinesin family member 18B (*KIF18B*), polo-like kinase 1 (*PLK1*), shugoshin 1 (*SGO1*), and shugoshin 1 (*SGO2*) (**Figure 5D**). Applying the combination of the two datasets, GO enrichment analysis indicated that the genes directly interacting with or related to KIF2C were mainly related to the biological processes of "mitotic nuclear division" and "chromosome segregation", the cellular component of "spindle" and "chromosome", and the molecular functions of "microtubule binding" and "tubulin binding". KEGG pathway analysis further suggested that the

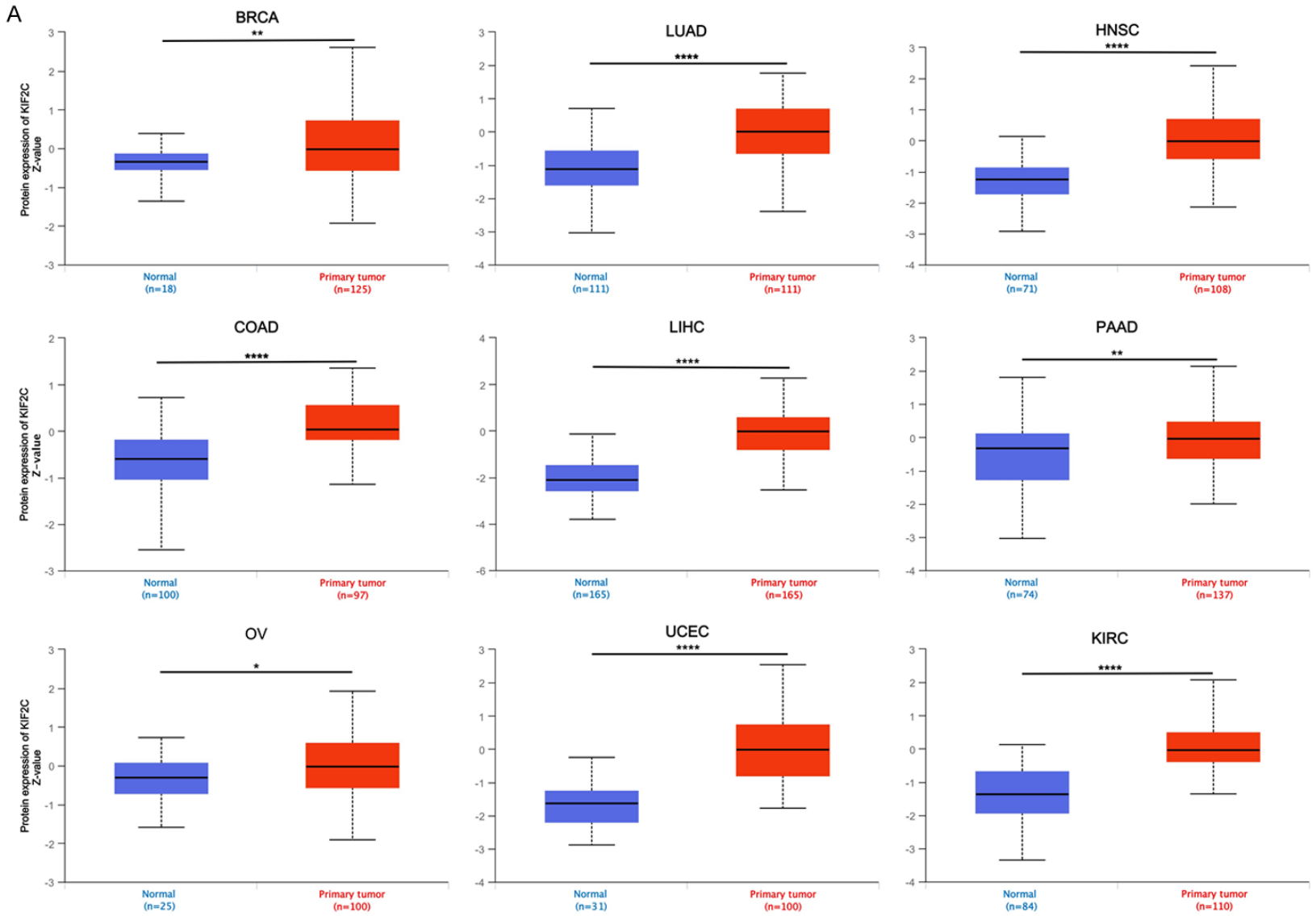
A
BRCA
**
LUAD
****
HNSC
****
COAD
****
LIHC
****
PAAD
**
OV
*
UCEC
****
KIRC
****
Protein expression of KIF2C Z-value
Normal (n=18)
Primary tumor (n=125)
Normal (n=111)
Primary tumor (n=111)
Normal (n=71)
Primary tumor (n=108)
Normal (n=100)
Primary tumor (n=97)
Normal (n=165)
Primary tumor (n=165)
Normal (n=74)
Primary tumor (n=137)
Normal (n=25)
Primary tumor (n=100)
Normal (n=31)
Primary tumor (n=100)
Normal (n=84)
Primary tumor (n=110)

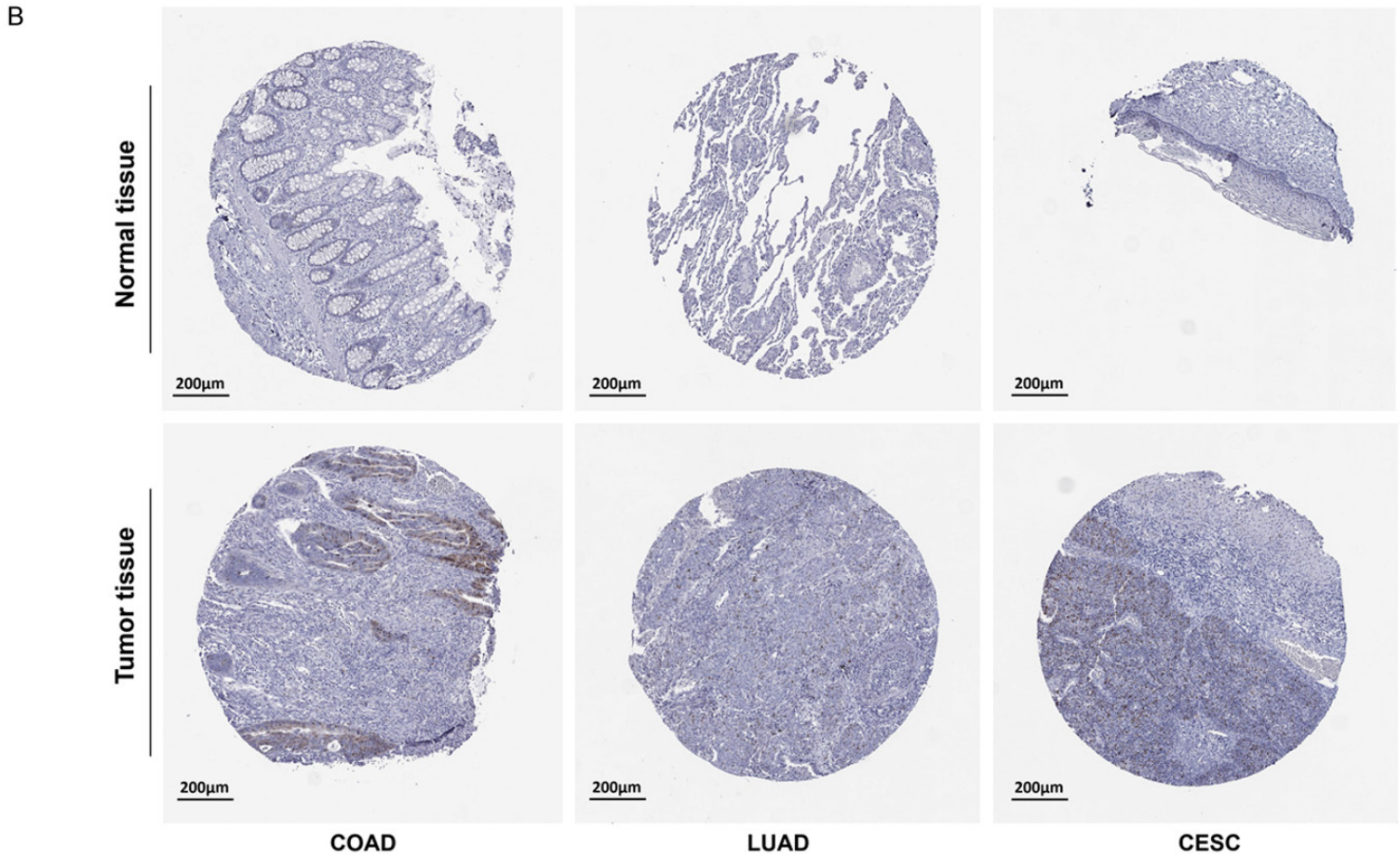

Figure 3. Protein expression of KIF2C in different tumors. A. The KIF2C total protein expression between normal tissue and primary tumor tissue according to the CPTAC database, Z-value represent standard deviations from the median across samples for the given cancer type. **P*<0.05, ***P*<0.01, ****P*<0.001, *****P*<0.0001, in Student's *t*-test. TPM, transcripts per million. B. KIF2C immunohistochemical staining images in human cancers compared with normal tissue from HPA database.

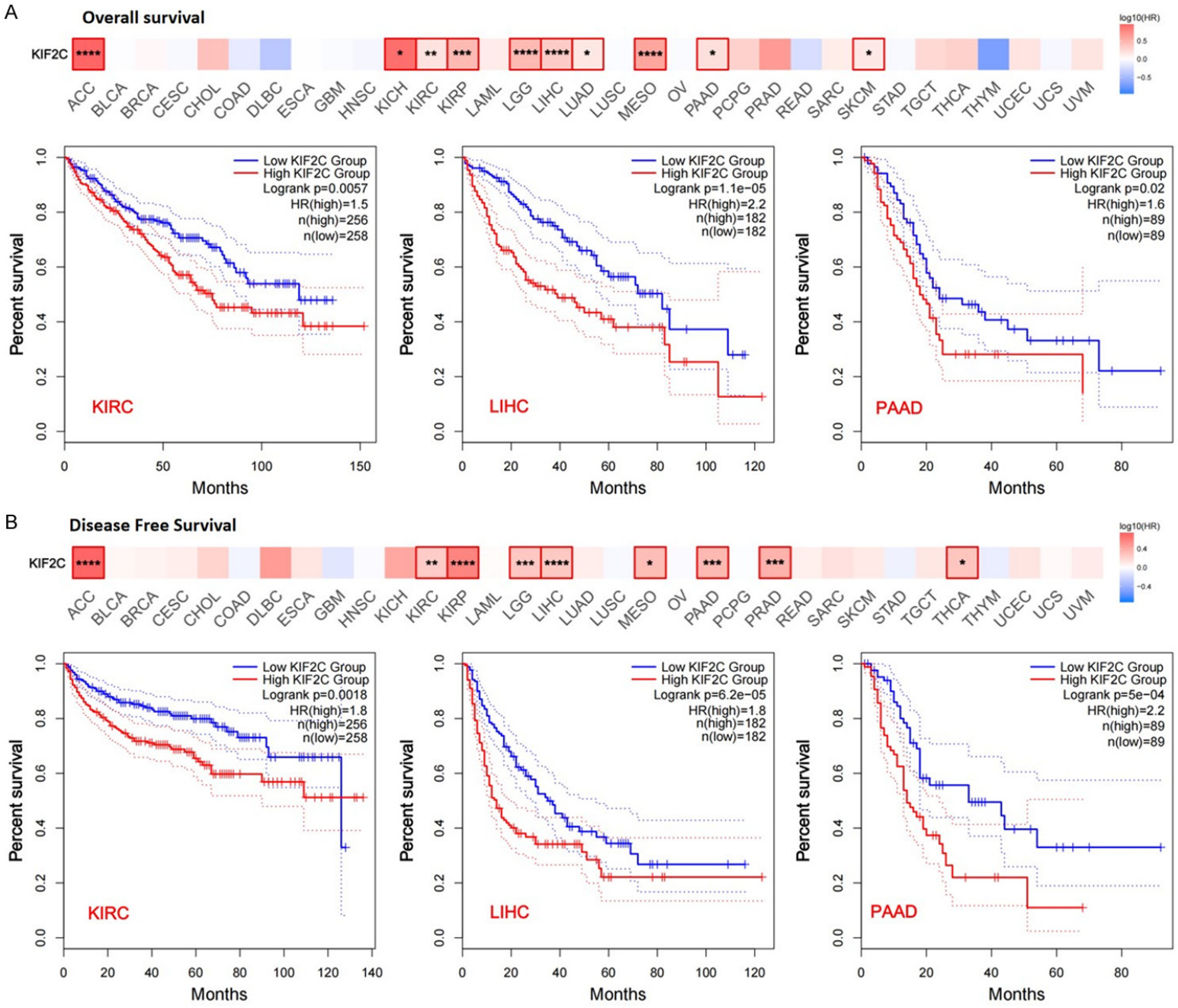
A
Overall survival
KIF2C
log10(HR)
ACC BLCA BRCA CESC CHOL COAD DLBC ESCA GBM HNSC KICH KIRC KIRP LAML LGG LIHC LUAD LUSC MESO OV PAAD PCPG PRAD READ SARC SKCM STAD TGCT THCA THYM UCEC UCS UVM
Low KIF2C Group
High KIF2C Group
Logrank p=0.0057
HR(high)=1.5
n(high)=256
n(low)=258
KIRC
Logrank p=1.1e−05
HR(high)=2.2
n(high)=182
n(low)=182
LIHC
Logrank p=0.02
HR(high)=1.6
n(high)=89
n(low)=89
PAAD
Percent survival
Months
B
Disease Free Survival
Logrank p=0.0018
HR(high)=1.8
n(high)=256
n(low)=258
Logrank p=6.2e−05
HR(high)=1.8
n(high)=182
n(low)=182
Logrank p=5e−04
HR(high)=2.2
n(high)=89
n(low)=89

Figure 4. Relations between KIF2C expression and survival prognosis of different tumors in TCGA database are shown in survival maps and Kaplan-Meier curves. GEPIA2 tool was used to obtain overall survival (A) and disease-free survival (B) analyses. Cutoff-high (50%) and cutoff-low (50%) values were used as the expression thresholds for separating the high-expression and low-expression cohorts. *P<0.05, **P<0.01, ***P<0.001, ****P<0.0001, in log-rank test. HR, hazard ratio.

"cell cycle" and "p53 signaling pathway" might be potential mechanisms underlying the effect of *KIF2C* on tumorigenesis (**Figure 5E**).

Gene set enrichment analysis data

MSigDB H (hallmark gene sets) and C6 (oncogenic gene sets) were analyzed in the present study. Enrichment of H analysis indicated that high expression of *KIF2C* was associated with genes involved in mitotic spindle assembly, cell cycle-related targets of E2F transcription factors, genes regulated by MYC, and genes regulated by KRAS (**Figure 6**). C6 enrichment analysis demonstrated that high expression of *KIF2C* was associated with various oncogenes such as E2F, EGFR, MYC, and KRAS (**Figure 7**).

Immune reactivities analysis data

Using the Sangerbox Estimate infiltration module, we determined the correlation of ImmunoScore, StromalScore, and ESTIMATEScore with *KIF2C* expression in 33 cancer types based on TCGA dataset (Table S4). *KIF2C* expression in GBM, UCEC, CESC, LUAD, SARC, STAD, LUSC, SKCM, and TGCT was significantly and negatively correlated with ImmunoScore, StromalScore, and ESTIMATEScore. In contrast, *KIF2C* expression in LGG, KIRC, and THCA was significantly and positively correlated with these three scores (**Figure 8A**). A negative correlation between KIF2C expression and ImmunoScore, StromalScore, and ESTIMATEScore was observed for GBM, STAD, and LUSC as shown in the representative scatter plots (**Figure 8B**). The correlation between the expression of *KIF2C* and infiltration level of MDSCs was estimated using TCGA dataset. Surprisingly, a significant and positive correlation between the expression of *KIF2C* and infiltration of MDSCs was observed in all cancer types, except HNSC-HPV+ and THCA (**Figure 8C**). A positive correlation between *KIF2C* expression and the infiltration estimation value was observed for GBM, STAD, and LUSC, as illustrated in the representative scatter plots (**Figure 8D**).

The immune checkpoint analysis demonstrated that the expression of *KIF2C* in most cancers was positively correlated with *CD276* and High Mobility Group Box 1 (*HMGB1*) (**Figure 9A**). Analysis of the relationship between *KIF2C* expression and MSI/TMB of cancers in TCGA cohort indicated that *KIF2C* expression was significantly and positively correlated with MSI in LUSC, PRAD, SARC, BRCA, COAD, STAD, and KICH, whereas it was negatively correlated with MSI in DLBC as illustrated in the radar chart (**Figure 9B**). The analysis also showed that *KIF2C* expression significantly and positively correlated with TMB in LUAD, PRAD, UCEC, TGCT, BRCA, COAD, STAD, SKCM, KIRC, READ, KICH, ACC, and PCPG (**Figure 9C**). Single-cell data demonstrated that KIF2C mainly expressed in malignant cells (**Figure 10**).

Experimental validation

To validate the KIF2C expression in human tumors, we verified bioinformatics data using qRT-PCR and western blot analysis to examine the RNA and protein levels of KIF2C in several gastric cancer cell lines. The results showed that KIF2C is highly expressed in SGC-7901, HGC-27, and MKN-45 when compared to GES-1 (**Figure 11A**, **11B**). In addition, the immunohistochemistry stainning demonstrated that KIF2C is positively expressed in STAD and LIHC when compared to adjacent normal tissues (**Figure 11C**, **11D**). However, there is no difference in KIF2C expression between the tumor tissues and adjacent normal lung tissues (**Figure 11E**).

Discussion

In the present study, we demonstrated that: 1) the expression level of *KIF2C* was significantly higher in tumor tissues than in normal tissues across most cancer types in TCGA cohort; 2) total KIF2C protein expression was higher in the primary cancers than in normal tissues for BRCA, COAD, LUAD, LIHC, HNSC, PAAD, KIRC, UCEC, and OV in the CPTAC dataset; 3) high expression of *KIF2C* was significantly associated with poor OS and DFS of various tumors in

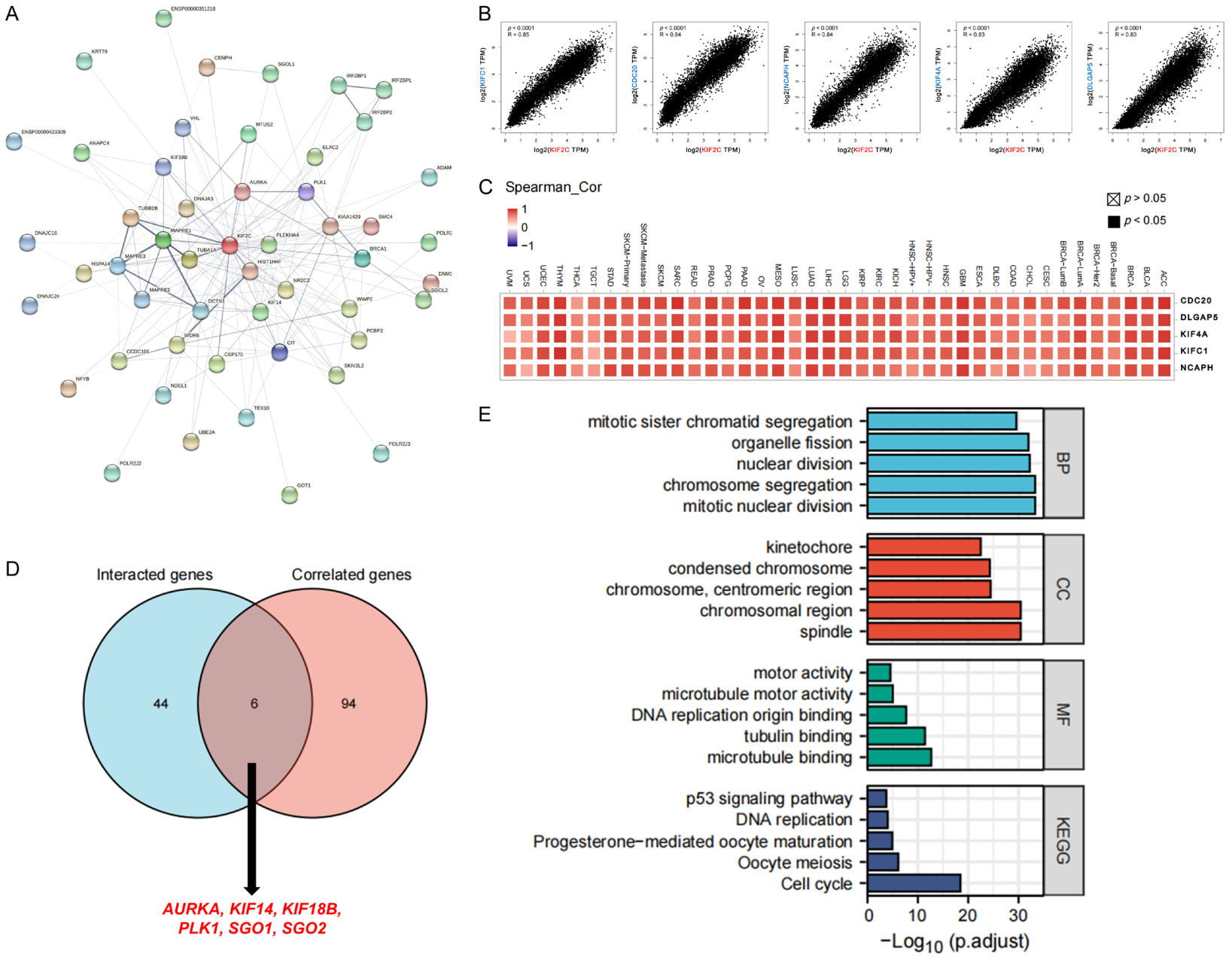
A
B
C
Spearman_Cor
p > 0.05
p < 0.05
CDC20
DLGAP5
KIF4A
KIFC1
NCAPH
D
Interacted genes
Correlated genes
44
6
94
AURKA, KIF14, KIF18B,
PLK1, SGO1, SGO2
E
mitotic sister chromatid segregation
organelle fission
nuclear division
chromosome segregation
mitotic nuclear division
BP
kinetochore
condensed chromosome
chromosome, centromeric region
chromosomal region
spindle
CC
motor activity
microtubule motor activity
DNA replication origin binding
tubulin binding
microtubule binding
MF
p53 signaling pathway
DNA replication
Progesterone−mediated oocyte maturation
Oocyte meiosis
Cell cycle
KEGG
0
10
20
30
−Log10 (p.adjust)

Figure 5. KIF2C related gene network, KEGG pathway analysis and GO enrichment analysis. A. 50 available experimentally determined KIF2C-interacted proteins using STRING tool. B. Top 100 *KIF2C*-correlated genes in TCGA database and selected targeting genes, including *CDC20*, *DLGAP5*, *KIF4A*, *KIFC1*, and *NCAPH*, in Pearson's correlation coefficient. C. The corresponding heatmap in the detailed tumor types, in purity-adjusted partial Spearman's rho. D. An intersection analysis of the KIF2C-interacted and *KIF2C*-correlated genes. E. The bar plot of GO enrichment analysis in biological process, molecular function, and cellular component. KEGG pathway analysis based on the KIF2C-interacted and *KIF2C*-correlated genes. Adjusted *p*-values were obtained from multiple hypotheses test using the Benjamini-Hochberg procedure, p.adjust <0.05 was considered statistically significant.

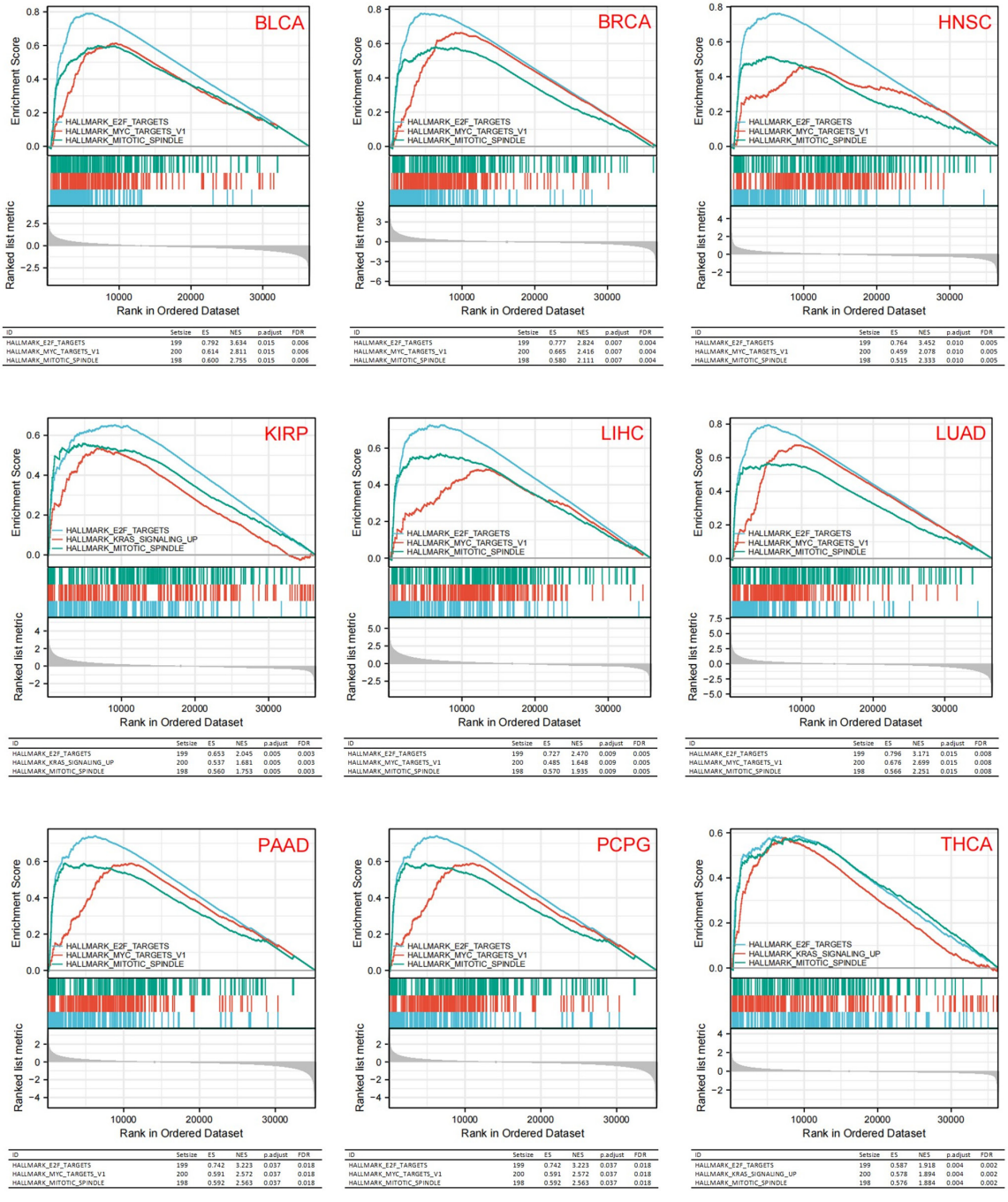

Figure 6. Hallmark Gene set enrichment analysis of KIF2C. Hallmark gene sets enriched in high *KIF2C* expression group. ES, enrichment score; NES, normalized enrichment score; FDR, false discovery rate.

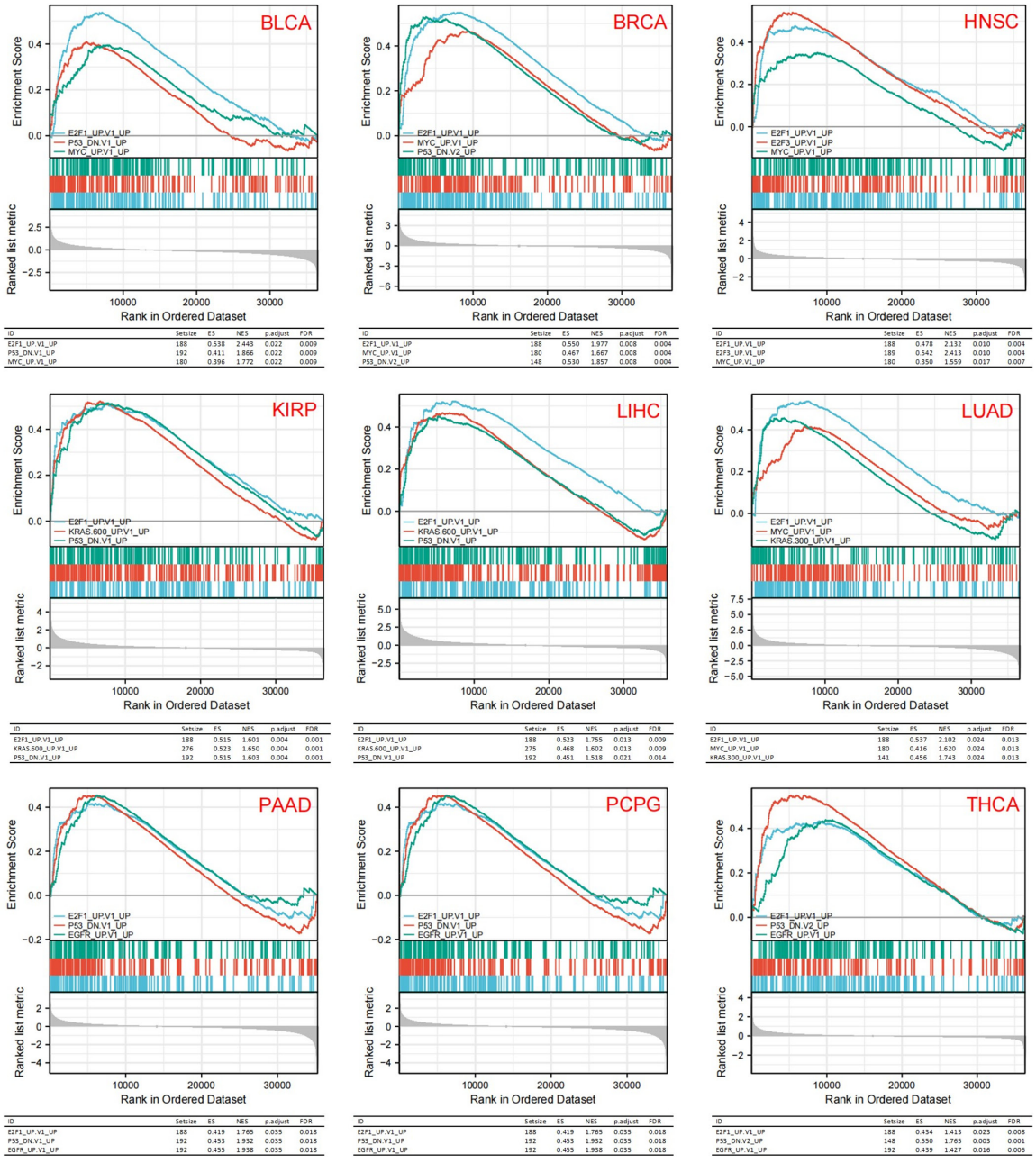

Figure 7. Oncogenic Gene set enrichment analysis of KIF2C. Oncogenic signature gene sets enriched in high *KIF2C* expression group. ES, enrichment score; NES, normalized enrichment score; FDR, false discovery rate.

TCGA database; 4) *KIF2C* was significantly and positively correlated with *KIFC1*, *CDC20*, *NCAPH*, *KIF4A*, and *DLGAP5* in all tumor types in TCGA cohort; 5) KEGG pathway analysis and GO enrichment analysis based on the *KIF2C*-interacted and -correlated genes showed that "cell cycle" and "p53 signaling pathway" might be the mechanisms for the effect of *KIF2C* on tumorigenesis; 6) high expression of *KIF2C* was significantly associated with *E2F*, *EGFR*, *MYC*, and *KRAS* signature oncogenes in BLCA, BRCA, HNSC, KIRP, LIHC, LUAD, PAAD, PCPG, and THCA; 7) *KIF2C* expression was significantly and negatively correlated with ImmunoScore, StromalScore, and ESTIMATEScore in most of the cancers in TCGA cohort; 8) a significant and positive correlation between the expression of *KIF2C* and infiltration of MDSCs was

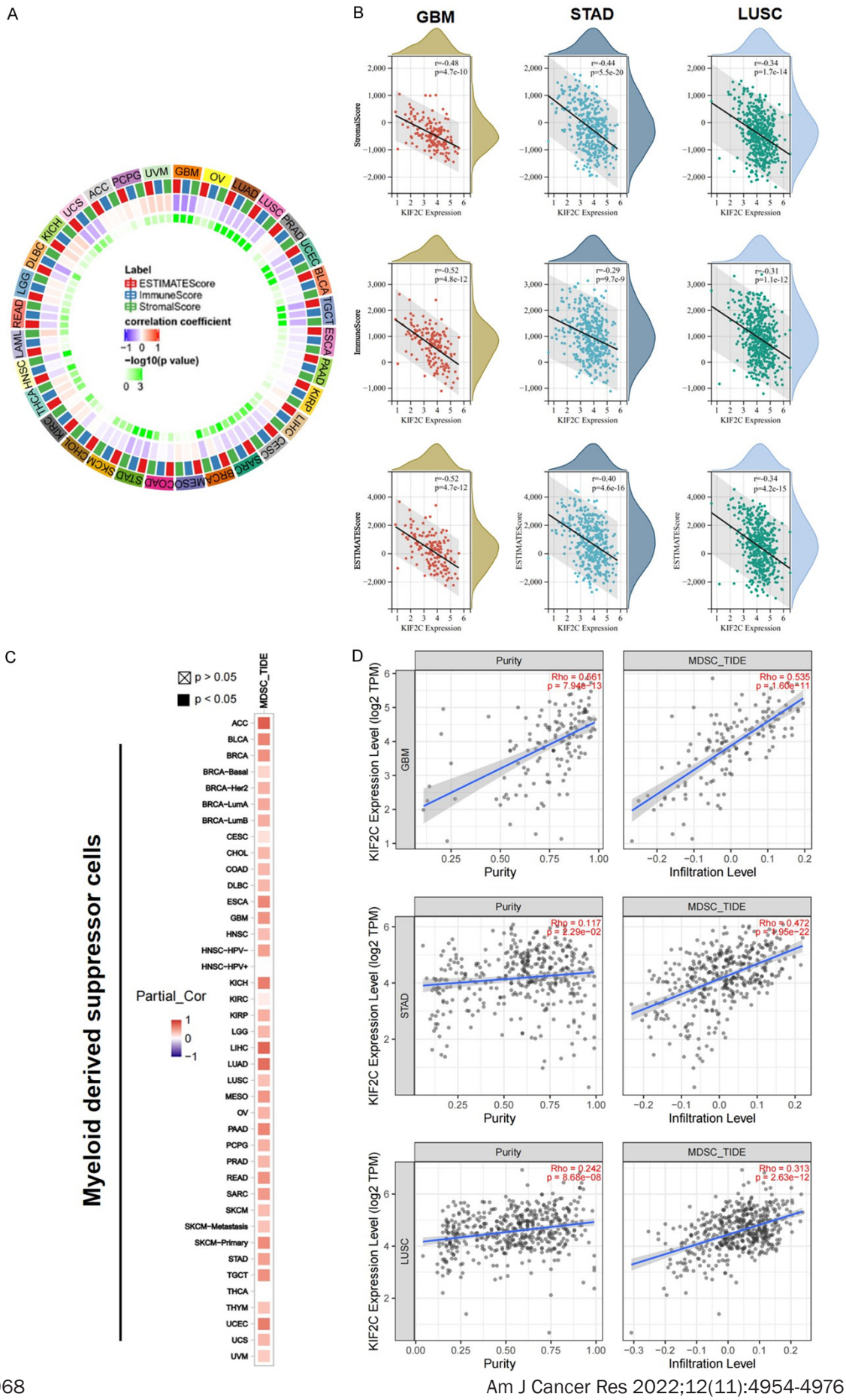
A
B
GBM
STAD
LUSC
C
D
Label
ESTIMATEScore
ImmuneScore
StromalScore
correlation coefficient
−log10(p value)
KIF2C Expression
StromalScore
ImmuneScore
ESTIMATEScore
r=-0.48
p=4.7e-10
r=-0.44
p=5.5e-20
r=-0.34
p=1.7e-14
r=-0.52
p=4.8e-12
r=-0.29
p=9.7e-9
r=-0.31
p=1.1e-12
r=-0.52
p=4.7e-12
r=-0.40
p=4.6e-16
r=-0.34
p=4.2e-15
p > 0.05
p < 0.05
MDSC_TIDE
Partial_Cor
Myeloid derived suppressor cells
Purity
MDSC_TIDE
KIF2C Expression Level (log2 TPM)
Infiltration Level
Rho = 0.661
p = 7.94e-73
Rho = 0.535
p = 1.60e-11
Rho = 0.117
p = 2.29e-02
Rho = 0.472
p = 1.95e-22
Rho = 0.242
p = 8.68e-08
Rho = 0.313
p = 2.63e-12

Figure 8. Immune reactivities analysis of KIF2C in different tumors of TCGA database. A, B. Correlation of ImmunoScore, StromalScore, and ESTIMATEScore with *KIF2C* expression in tumors, in Pearson's correlation coefficient. C, D. Correlation analysis between *KIF2C* expression and immune infiltration of myeloid derived suppressor cells, in purity-adjusted Spearman's rho, with TIDE algorithm. TIDE, tumor immune dysfunction and exclusion.

present in all tumor types except for HNSC-HPV+ and THCA; 9) *KIF2C* expression was significantly and positively correlated with MSI, TMB, *CD276*, and *HMGB1* immune checkpoints in most of the cancers in TCGA cohort.

KIF2C is the best-characterized member of the kinesin-13 family, and is involved in the fine-tuned dynamics of mitotic spindles, and reductions in kinetochore-microtubule turnover induce severe chromosome segregation defects [2]. Previous studies have shown that KIF2C is highly expressed and associated with poor prognosis for LIHC, STAD, and COAD [8, 9, 15]. A recent study showed that KIF2C acts as a key factor in mediating the crosstalk between Wnt/β-catenin and mTORC1 signaling and promotes LIHC cell proliferation, migration, invasion, and metastasis both *in vitro* and *in vivo* [8]. In addition, KIF2C expression was significantly suppressed by ectopic introduction of p53 [16]. The present study also showed that *KIF2C* expression was significantly increased in most tumors in TCGA dataset and was related to poor prognosis. These data demonstrate that the expression of KIF2C could lead to tumorigenesis and cancer metastasis in a variety of tumors, warranting further investigation.

Among the top 100 genes with similar expression patterns as *KIF2C* in the tumors of TCGA cohort, *KIF2C* expression was significantly and positively correlated with *KIFC1*, *CDC20*, *NCAPH*, *KIF4A*, and *DLGAP5* expression in all tumor types in TCGA database. Although there is no physical interaction between *KIF2C* and these five genes, these genes are all involved in "cell cycle" and "p53 signaling pathway". KIFC1 drives chromosome segregation errors and aneuploidy, resulting in tumorigenesis initiation and/or acceleration [17]. The oncogenic role of CDC20 has been reported in various human cancers, including PAAD, BRCA, PRAD, COAD, LUAD, and LIHC [18]. Although NCAPH plays a central role in mitotic chromosome assembly and segregation in humans [19], there is little data on the relationship between NCAPH and cancer in the literature. A recent study showed that KIF4A drives aggressive PRAD phenotypes and is associated with poor outcome [20]. circKIF4A has been demonstrated to be a prognostic factor and mediator that regulates the progression of triple-negative breast cancer [21]. Pan-cancer analysis showed that DLGAP5 is highly expressed in most types of cancers and is associated with poor prognosis [22].

Using the data for both KIF2C-interacted proteins and *KIF2C*-correlated genes, KEGG pathway analysis showed that targeting the cell cycle and p53 signaling pathway might be important mechanisms for the effect of *KIF2C* on tumorigenesis. GO enrichment analysis further suggested that the genes directly interacting with or related to *KIF2C* were mainly related to mitotic nuclear division and chromosome segregation. GSEA for the hallmark gene sets demonstrated that high expression of *KIF2C* was associated with genes involved in mitotic spindle assembly in various tumors of TCGA cohort. As KIF2C is involved in both spindle formation and regulation of DNA double-strand breaks, precise regulation of KIF2C is essential to prevent malignant transformation associated with gains or losses of DNA content [6]. Thus, perturbations in KIF2C may lead to chromosomal instability and aneuploidy. In the present study, intersection analysis of KIF2C-interacted proteins and *KIF2C*-correlated genes identified six genes *AURKA*, *KIF14*, *KIF18B*, *PLK1*, *SGO1*, and *SGO2*, which are potentially important regulatory molecules associated with KIF2C for tumorigenesis. Indeed, the interactions between KIF2C and AURKA, and between KIF2C and PLK1 have been detected using enzymatic assays [23, 24]. Kinases such as AURKA and PLK1 are often deregulated in cancer cells, leading to perturbations in the proper regulation of KIF2C, which in turn could enhance mitotic defects [25]. In addition, the interaction between KIF2C and KIF14, and between KIF2C and KIF18B has been detected using affinity chromatography technology assays [26, 27]. AURKA regulates spindle microtubule dynamics through the KIF2C-KIF18B complex [28]. A study showed that the interaction between KIF2C and SGO1 was detected by an anti-tag co-immunoprecipita-

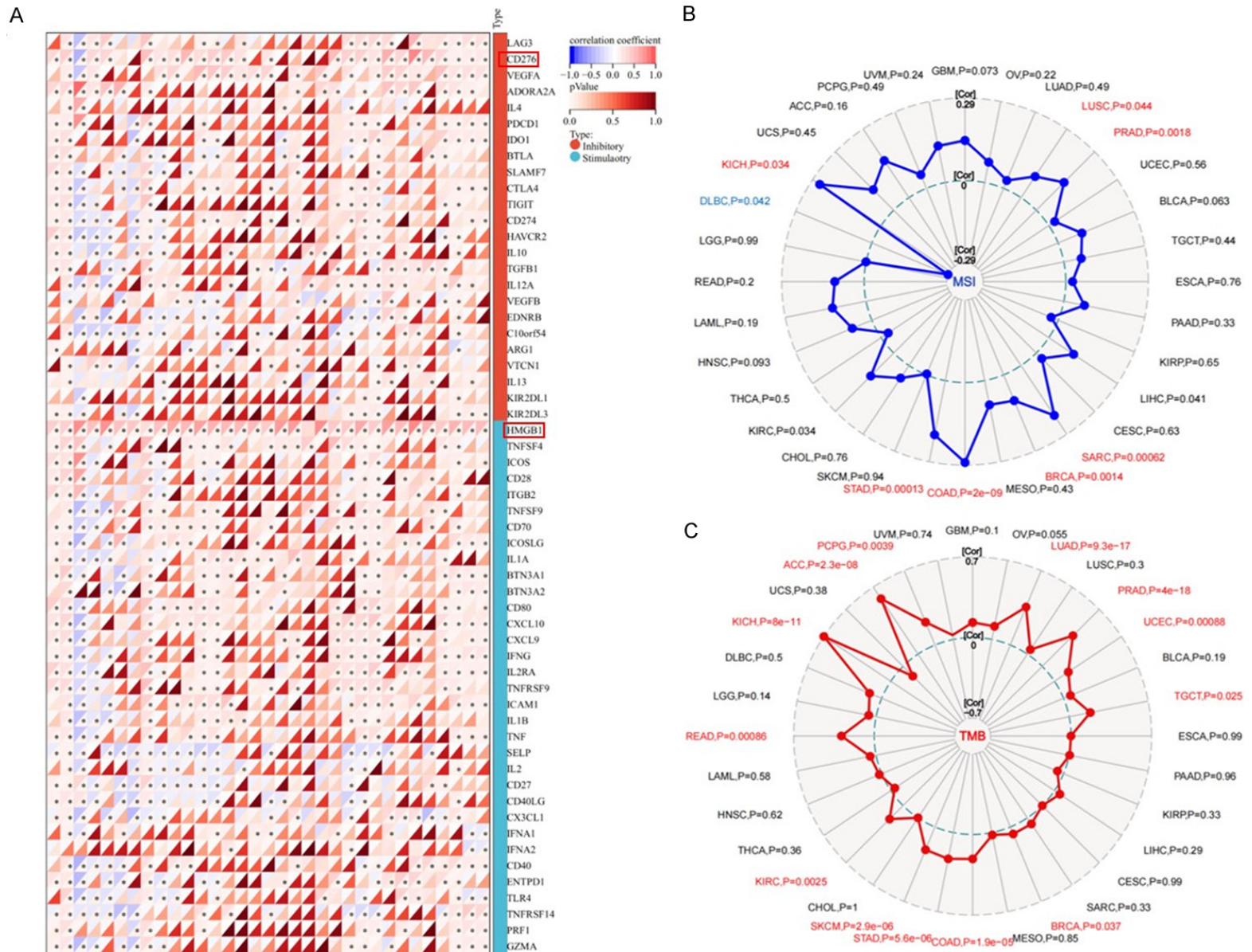
A
Type
correlation coefficient
−1.0 −0.5 0.0 0.5 1.0
pValue
0.0 0.5 1.0
Type:
Inhibitory
Stimulaotry
LAG3
CD276
VEGFA
ADORA2A
IL4
PDCD1
IDO1
BTLA
SLAMF7
CTLA4
TIGIT
CD274
HAVCR2
IL10
TGFB1
IL12A
VEGFB
EDNRB
C10orf54
ARG1
VTCN1
IL13
KIR2DL1
KIR2DL3
HMGB1
TNFSF4
ICOS
CD28
ITGB2
TNFSF9
CD70
ICOSLG
IL1A
BTN3A1
BTN3A2
CD80
CXCL10
CXCL9
IFNG
IL2RA
TNFRSF9
ICAM1
IL1B
TNF
SELP
IL2
CD27
CD40LG
CX3CL1
IFNA1
IFNA2
CD40
ENTPD1
TLR4
TNFRSF14
PRF1
GZMA
CCL5
TNFRSF18
TNFRSF4
LGG(N=509)
LIHC(N=369)
OV(N=410)
PAAD(N=178)
UVM(N=79)
KIRC(N=530)
LUSC(N=498)
UCEC(N=180)
ESCA(N=181)
STAD(N=414)
SKCM(N=102)
READ(N=92)
CESC(N=304)
SARC(N=258)
LAML(N=173)
CHOL(N=36)
DLBC(N=47)
MESO(N=87)
LUAD(N=513)
BLCA(N=407)
BRCA(N=1092)
ACC(N=77)
PCPG(N=177)
KICH(N=66)
KIRP(N=288)
HNSC(N=518)
COAD(N=288)
PRAD(N=495)
THCA(N=504)
THYM(N=119)
GBM(N=153)
TGCT(N=148)
UCS(N=57)
B
MSI
[Cor]
0.29
[Cor]
0
[Cor]
-0.29
UVM,P=0.24
GBM,P=0.073
OV,P=0.22
PCPG,P=0.49
LUAD,P=0.49
ACC,P=0.16
LUSC,P=0.044
UCS,P=0.45
PRAD,P=0.0018
KICH,P=0.034
UCEC,P=0.56
DLBC,P=0.042
BLCA,P=0.063
LGG,P=0.99
TGCT,P=0.44
READ,P=0.2
ESCA,P=0.76
LAML,P=0.19
PAAD,P=0.33
HNSC,P=0.093
KIRP,P=0.65
THCA,P=0.5
LIHC,P=0.041
KIRC,P=0.034
CESC,P=0.63
CHOL,P=0.76
SARC,P=0.00062
SKCM,P=0.94
BRCA,P=0.0014
STAD,P=0.00013
COAD,P=2e−09
MESO,P=0.43
C
TMB
[Cor]
0.7
[Cor]
0
[Cor]
−0.7
UVM,P=0.74
GBM,P=0.1
OV,P=0.055
PCPG,P=0.0039
LUAD,P=9.3e−17
ACC,P=2.3e−08
LUSC,P=0.3
UCS,P=0.38
PRAD,P=4e−18
KICH,P=8e−11
UCEC,P=0.00088
DLBC,P=0.5
BLCA,P=0.19
LGG,P=0.14
TGCT,P=0.025
READ,P=0.00086
ESCA,P=0.99
LAML,P=0.58
PAAD,P=0.96
HNSC,P=0.62
KIRP,P=0.33
THCA,P=0.36
LIHC,P=0.29
KIRC,P=0.0025
CESC,P=0.99
CHOL,P=1
SARC,P=0.33
SKCM,P=2.9e−06
BRCA,P=0.037
STAD,P=5.6e−06
COAD,P=1.9e−05
MESO,P=0.85

Figure 9. Correlation of KIF2C expression with immune checkpoints, MSI, and TMB in TCGA database. A. Heatmap represents the color-coded correlations of immune checkpoints and KIF2C across different tumors. B. Radar chart displays the overlap between KIF2C and MSI. C. Radar chart displays the overlap between KIF2C and TMB. **P*<0.05, ***P*<0.01, ****P*<0.001, in Pearson's correlation coefficient.

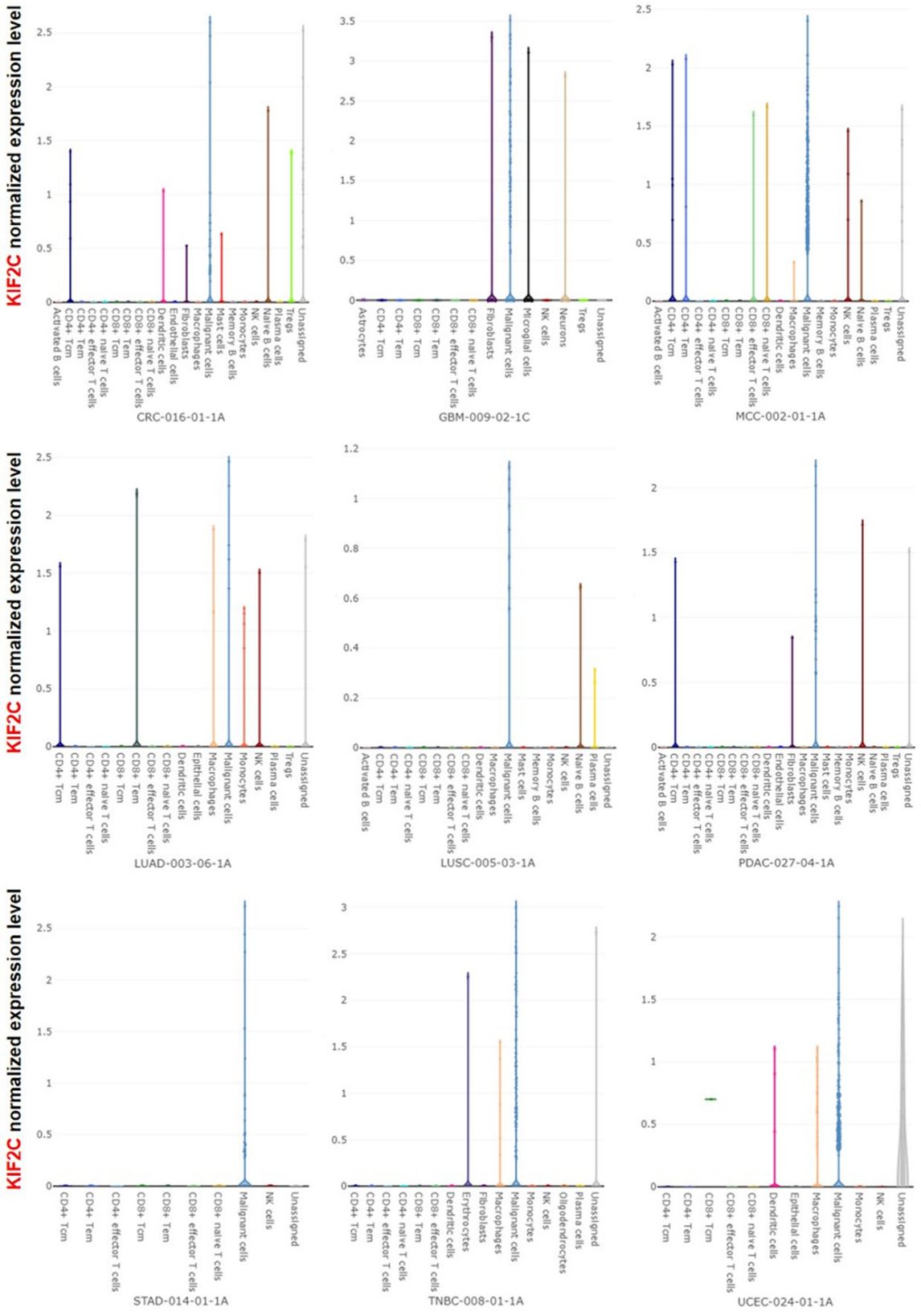

Figure 10. Single-cell data analysis of KIF2C expression in Cancer Single-cell Expression Map. KIF2C expression in malignant cells and various immune cells. CRC, colorectal cancer; MCC, Merkel cell carcinoma; PDAC, pancreatic ductal adenocarcinoma; TNBC, triple-negative breast cancer.

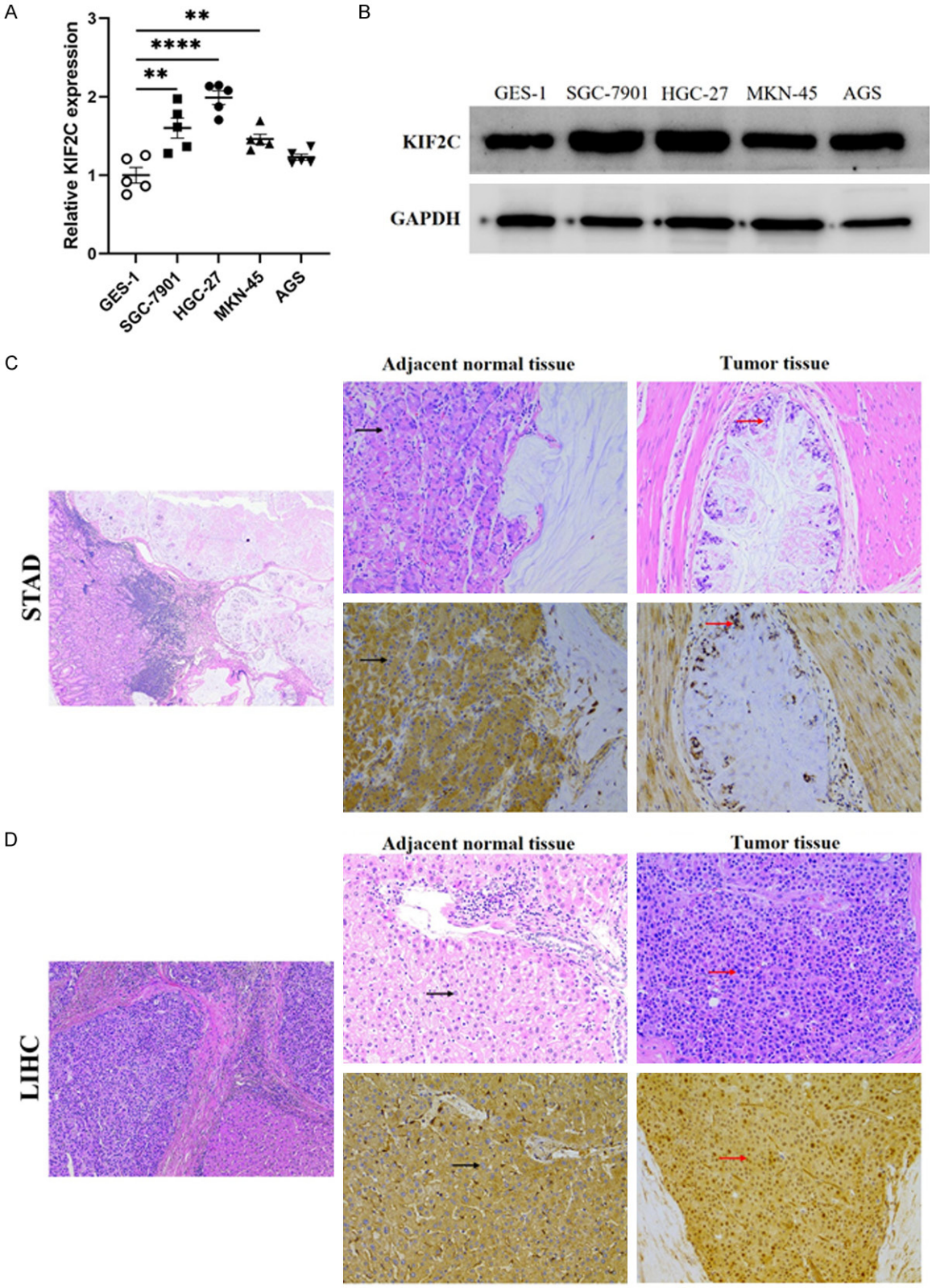

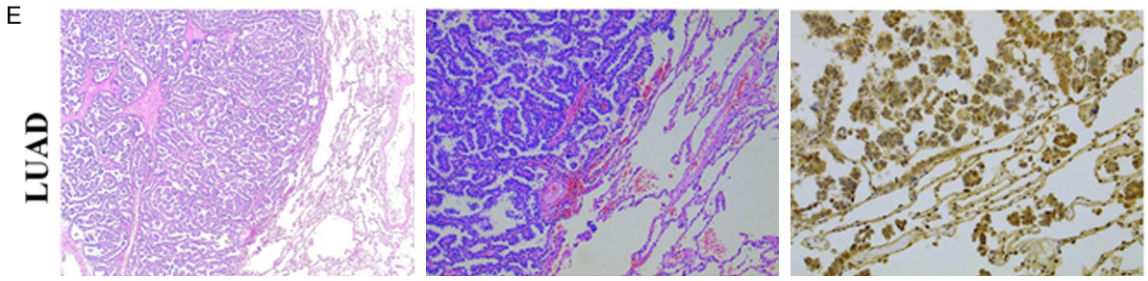

Figure 11. KIF2C is highly expressed in gastric cancer cell lines, STAD, and LIHC. A. *KIF2C* expression in human gastric cancer cell lines analyzed by real-time PCR. B. KIF2C expression in human gastric cancer cell lines analyzed by western blot. C-E. KIF2C immunohistochemical staining images in human cancers compared with adjacent normal tissue. The red arrow showed positive expression of KIF2C in the nucleus of tumor cells. $^{**}P<0.01$ and $^{****}P<0.0001$ in Student's *t*-test.

tion assay [29], but no further study has investigated the effect of SGO1 on the regulation of KIF2C. Indeed, SGO1 downregulation leads to chromosomal instability in COAD [30], and it is reasonable to hypothesize that SGO1 downregulation through KIF2C leads to chromosomal instability. The interaction between KIF2C and SGO2 has been detected using anti-bait co-immunoprecipitation assay [31], and phosphorylation of SGO2 is essential for localizing KIF2C to centromeres [32]. However, it is unclear whether the interactions between KIF2C, KIF14, KIF18B, SGO1, and SGO2 have synergistic effects on cancer progression. In this study, GSEA showed that high expression of KIF2C was associated with the oncogenic signatures such as E2F, EGFR, MYC, and KRAS. Notably, the roles of E2F, EGFR, MYC and KRAS in cancer have been extensively studied [33-36].

In the present study, we observed a significant and positive correlation between the expression of *KIF2C* and infiltration of MDSCs in all tumor types except for HNSC-HPV+ and THCA, while expression of *KIF2C* negatively correlated with ImmunoScore, which has been used to quantify the in situ T cell infiltration in most of the tumors in the TCGA cohort. In addition, single-cell data shows that KIF2C is mainly expressed in malignant cells. MDSCs are immunomodulatory cells that suppress adaptive immune responses and promote tumor progression and metastasis and are involved in multidrug resistance [37, 38]. A clinical study has shown that increased MDSC levels in patients with recurrent GBM are associated with poor prognosis [39]. It has been reported that MDSCs produce eotaxin-1 to promote LUSC metastasis via activation of ERK and AKT signaling [40]. A clinical study has suggested that patients with STAD have higher levels of circulating MDSCs than healthy individuals, and high levels of MDSCs are correlated with advanced cancer stage and reduced survival [41]. These data support the hypothesis that KIF2C overexpression in cancer cells may recruit more MDSCs, not T cells, to infiltrate the tumor microenvironment, thus leading to poor prognosis.

Immunotherapy is an evolving cancer treatment that helps the immune system fight cancer. Among the most promising approaches to activate therapeutic antitumor immunity is blocking immune checkpoints [42]. *KIF2C* is positively correlated with most of the immune checkpoint genes in tumors of TCGA cohort, especially *CD276* and *HMGB1*. CD276 is highly expressed in a wide range of human cancers and plays an important role in the inhibition of T-cell functions [43]. HMGB1 plays both oncogenic and tumor-suppressive roles during tumor development and therapy [44]. Unfortunately, many patients with a positive initial response later develop resistance to immune checkpoint inhibitors [45]. Notably, MDSCs can blunt the anticancer activity of immune checkpoint inhibitors [46]. Indeed, HMGB1 inhibition drastically reduces MDSCs and improves the efficacy of anti-PD-1 cancer monoimmunotherapy [47]. Both MSI and TMB are promising predictive biomarkers for the efficacy of immune checkpoint inhibitors in cancer treatment [48]. The findings of the present study suggest that *KIF2C* expression is significantly and positively correlated with MSI and TMB in a portion of tumors in TCGA cohort.

KIF2C depletion or inhibition of its microtubule depolymerase activity impairs the formation of DNA damage foci and reduces the mobility of DNA double-strand breaks [6], suggesting that KIF2C may be an attractive therapeutic target for human cancers. UMK57 is a novel chromosomal instability inhibitor that potentiates KIF2C *in vivo* and transiently suppresses chromosome mis-segregation in cancer cells with chromosomal instability, while cancer cells with chromosomal instability display adaptive resistance to UMK57 [49]. Rigosertib, a non-ATP-competitive inhibitor of PLK1, kills cancer cells via microtubule destabilization [50]. Indeed, *KIF2C* overexpression enhances microtubule destabilization by rigosertib [51], indicating that rigosertib could be an effective antitumor drug among patients with KIF2C highly expressed cancer.

In conclusion, the present pan-cancer analyses of KIF2C revealed that KIF2C expression was correlated with oncogenic signature gene sets, MDSC infiltration, ImmunoScore, immune checkpoints, MSI, TMB, and clinical prognosis across multiple tumors. These data may aid in the understanding of the role of KIF2C in tumorigenesis and immunotherapy.

Disclosure of conflict of interest

None.

Address correspondence to: Dr. Hao Wu, Department of Gastroenterology, Third Xiangya Hospital, Central South University, 138 Tongzipo Road, Changsha 4100013, Hunan, China. E-mail: xiangyawuhao@csu.edu.cn; Dr. Xiaoyang Pang, Department of Orthopaedics, Xiangya Hospital, Central South University, 87 Xiangya Road, Changsha 410008, Hunan, China. E-mail: xiaoyangpang@csu.edu.cn

References

[1] Zhang B, Li Y, Pang X and Wu H. Bioinformatics analysis of kinesin family member 2C in human tumors: novel prognostic biomarker and tumor microenvironment regulator. ResearchSquare. 2022. Avialble from: https://doi.org/10.21203/rs.3.rs-1475809/v2.

[2] Bakhoum SF, Thompson SL, Manning AL and Compton DA. Genome stability is ensured by temporal control of kinetochore-microtubule dynamics. Nat Cell Biol 2009; 11: 27-35.

[3] Andrews PD, Ovechkina Y, Morrice N, Wagenbach M, Duncan K, Wordeman L and Swedlow JR. Aurora B regulates MCAK at the mitotic centromere. Dev Cell 2004; 6: 253-68.

[4] Wang W, Cantos-Fernandes S, Lv Y, Kuerban H, Ahmad S, Wang C and Gigant B. Insight into microtubule disassembly by kinesin-13s from the structure of Kif2C bound to tubulin. Nat Commun 2017; 8: 70.

[5] Bakhoum SF and Compton DA. Chromosomal instability and cancer: a complex relationship with therapeutic potential. J Clin Invest 2012; 122: 1138-43.

[6] Zhu S, Paydar M, Wang F, Li Y, Wang L, Barrette B, Bessho T, Kwok BH and Peng A. Kinesin Kif2C in regulation of DNA double strand break dynamics and repair. Elife 2020; 9: e53402.

[7] Eichenlaub-Ritter U, Staubach N and Trapphoff T. Chromosomal and cytoplasmic context determines predisposition to maternal age-related aneuploidy: brief overview and update on MCAK in mammalian oocytes. Biochem Soc Trans 2010; 38: 1681-6.

[8] Wei S, Dai M, Zhang C, Teng K, Wang F, Li H, Sun W, Feng Z, Kang T, Guan X, Xu R, Cai M and Xie D. KIF2C: a novel link between Wnt/β-catenin and mTORC1 signaling in the pathogenesis of hepatocellular carcinoma. Protein Cell 2021; 12: 788-809.

[9] Ishikawa K, Kamohara Y, Tanaka F, Haraguchi N, Mimori K, Inoue H and Mori M. Mitotic centromere-associated kinesin is a novel marker for prognosis and lymph node metastasis in colorectal cancer. Br J Cancer 2008; 98: 1824-9.

[10] Gao J, Aksoy BA, Dogrusoz U, Dresdner G, Gross B, Sumer SO, Sun Y, Jacobsen A, Sinha R, Larsson E, Cerami E, Sander C and Schultz N. Integrative analysis of complex cancer genomics and clinical profiles using the cBioPortal. Sci Signal 2013; 6: pl1.

[11] Tang Z, Kang B, Li C, Chen T and Zhang Z. GEPIA2: an enhanced web server for large-scale expression profiling and interactive analysis. Nucleic Acids Res 2019; 47: W556-W560.

[12] Ghandi M, Huang FW, Jané-Valbuena J, Kryukov GV, Lo CC, McDonald ER 3rd, Barretina J, Gelfand ET, Bielski CM, Li H, Hu K, Andreev-Drakhlin AY, Kim J, Hess JM, Haas BJ, Aguet F, Weir BA, Rothberg MV, Paolella BR, Lawrence MS, Akbani R, Lu Y, Tiv HL, Gokhale PC, de Weck A, Mansour AA, Oh C, Shih J, Hadi K, Rosen Y, Bistline J, Venkatesan K, Reddy A, Sonkin D, Liu M, Lehar J, Korn JM, Porter DA, Jones MD, Golji J, Caponigro G, Taylor JE, Dunning CM, Creech AL, Warren AC, McFarland JM, Zamanighomi M, Kauffmann A, Stransky N, Imielinski M, Maruvka YE, Cherniack AD, Tsherniak A, Vazquez F, Jaffe JD, Lane AA,

Weinstock DM, Johannessen CM, Morrissey MP, Stegmeier F, Schlegel R, Hahn WC, Getz G, Mills GB, Boehm JS, Golub TR, Garraway LA and Sellers WR. Next-generation characterization of the cancer cell line encyclopedia. Nature 2019; 569: 503-8.

[13] Chen F, Chandrashekar DS, Varambally S and Creighton CJ. Pan-cancer molecular subtypes revealed by mass-spectrometry-based proteomic characterization of more than 500 human cancers. Nat Commun 2019; 10: 5679.

[14] Zeng J, Zhang Y, Shang Y, Mai J, Shi S, Lu M, Bu C, Zhang Z, Zhang Z, Li Y, Du Z and Xiao J. CancerSCEM: a database of single-cell expression map across various human cancers. Nucleic Acids Res 2022; 50: D1147-D1155.

[15] Nakamura Y, Tanaka F, Haraguchi N, Mimori K, Matsumoto T, Inoue H, Yanaga K and Mori M. Clinicopathological and biological significance of mitotic centromere-associated kinesin overexpression in human gastric cancer. Br J Cancer 2007; 97: 543-9.

[16] Shimo A, Tanikawa C, Nishidate T, Lin ML, Matsuda K, Park JH, Ueki T, Ohta T, Hirata K, Fukuda M, Nakamura Y and Katagiri T. Involvement of kinesin family member 2C/mitotic centromere-associated kinesin overexpression in mammary carcinogenesis. Cancer Sci 2008; 99: 62-70.

[17] Basto R, Brunk K, Vinadogrova T, Peel N, Franz A, Khodjakov A and Raff JW. Centrosome amplification can initiate tumorigenesis in flies. Cell 2008; 133: 1032-42.

[18] Wang L, Zhang J, Wan L, Zhou X, Wang Z and Wei W. Targeting Cdc20 as a novel cancer therapeutic strategy. Pharmacol Ther 2015; 151: 141-51.

[19] Ono T, Losada A, Hirano M, Myers MP, Neuwald AF and Hirano T. Differential contributions of condensin I and condensin II to mitotic chromosome architecture in vertebrate cells. Cell 2003; 115: 109-21.

[20] Das R, Sjöström M, Shrestha R, Yogodzinski C, Egusa EA, Chesner LN, Chen WS, Chou J, Dang DK, Swinderman JT, Ge A, Hua JT, Kabir S, Quigley DA, Small EJ, Ashworth A, Feng FY and Gilbert LA. An integrated functional and clinical genomics approach reveals genes driving aggressive metastatic prostate cancer. Nat Commun 2021; 12: 4601.

[21] Tang H, Huang X, Wang J, Yang L, Kong Y, Gao G, Zhang L, Chen ZS and Xie X. circKIF4A acts as a prognostic factor and mediator to regulate the progression of triple-negative breast cancer. Mol Cancer 2019; 18: 23.

[22] Tang N, Dou X, You X, Shi Q, Ke M and Liu G. Pan-cancer analysis of the oncogenic role of discs large homolog associated protein 5 (DLGAP5) in human tumors. Cancer Cell Int 2021; 21: 457.

[23] Zhang X, Ems-McClung SC and Walczak CE. Aurora A phosphorylates MCAK to control ran-dependent spindle bipolarity. Mol Biol Cell 2008; 19: 2752-65.

[24] Sanhaji M, Ritter A, Belsham HR, Friel CT, Roth S, Louwen F and Yuan J. Polo-like kinase 1 regulates the stability of the mitotic centromere-associated kinesin in mitosis. Oncotarget 2014; 5: 3130-44.

[25] Ritter A, Kreis NN, Louwen F, Wordeman L and Yuan J. Molecular insight into the regulation and function of MCAK. Crit Rev Biochem Mol Biol 2015; 51: 228-45.

[26] Boldt K, van Reeuwijk J, Lu Q, Koutroumpas K, Nguyen TM, Texier Y, van Beersum SE, Horn N, Willer JR, Mans DA, Dougherty G, Lamers IJ, Coene KL, Arts HH, Betts MJ, Beyer T, Bolat E, Gloeckner CJ, Haidari K, Hetterschijt L, Iaconis D, Jenkins D, Klose F, Knapp B, Latour B, Letteboer SJ, Marcelis CL, Mitic D, Morleo M, Oud MM, Riemersma M, Rix S, Terhal PA, Toedt G, van Dam TJ, de Vrieze E, Wissinger Y, Wu KM, Apic G, Beales PL, Blacque OE, Gibson TJ, Huynen MA, Katsanis N, Kremer H, Omran H, van Wijk E, Wolfrum U, Kepes F, Davis EE, Franco B, Giles RH, Ueffing M, Russell RB and Roepman R; UK10K Rare Diseases Group. An organelle-specific protein landscape identifies novel diseases and molecular mechanisms. Nat Commun 2016; 7: 11491.

[27] Capalbo L, Bassi ZI, Geymonat M, Todesca S, Copoiu L, Enright AJ, Callaini G, Riparbelli MG, Yu L, Choudhary JS, Ferrero E, Wheatley S, Douglas ME, Mishima M and D'Avino PP. The midbody interactome reveals unexpected roles for PP1 phosphatases in cytokinesis. Nat Commun 2019; 10: 4513.

[28] Tanenbaum ME, Macurek L, van der Vaart B, Galli M, Akhmanova A and Medema RH. A complex of Kif18b and MCAK promotes microtubule depolymerization and is negatively regulated by Aurora kinases. Curr Biol 2011; 21: 1356-65.

[29] Hein MY, Hubner NC, Poser I, Cox J, Nagaraj N, Toyoda Y, Gak IA, Weisswange I, Mansfeld J, Buchholz F, Hyman AA and Mann M. A human interactome in three quantitative dimensions organized by stoichiometries and abundances. Cell 2015; 163: 712-23.

[30] Iwaizumi M, Shinmura K, Mori H, Yamada H, Suzuki M, Kitayama Y, Igarashi H, Nakamura T, Suzuki H, Watanabe Y, Hishida A, Ikuma M and Sugimura H. Human Sgo1 downregulation leads to chromosomal instability in colorectal cancer. Gut 2009; 58: 249-60.

[31] Orth M, Mayer B, Rehm K, Rothweiler U, Heidmann D, Holak TA and Stemmann O. Shu-

goshin is a Mad1/Cdc20-like interactor of Mad2. EMBO J 2011; 30: 2868-80.
[32] Tanno Y, Kitajima TS, Honda T, Ando Y, Ishiguro K and Watanabe Y. Phosphorylation of mammalian Sgo2 by Aurora B recruits PP2A and MCAK to centromeres. Genes Dev 2010; 24: 2169-79.
[33] Kent LN and Leone G. The broken cycle: E2F dysfunction in cancer. Nat Rev Cancer 2019; 19: 326-38.
[34] Ciardiello F and Tortora G. EGFR antagonists in cancer treatment. N Engl J Med 2008; 358: 1160-74.
[35] Gabay M, Li Y and Felsher DW. MYC activation is a hallmark of cancer initiation and maintenance. Cold Spring Harb Perspect Med 2014; 4: a014241.
[36] Uprety D and Adjei AA. KRAS: from undruggable to a druggable cancer target. Cancer Treat Rev 2020; 89: 102070.
[37] Gabrilovich DI and Nagaraj S. Myeloid-derived suppressor cells as regulators of the immune system. Nat Rev Immunol 2009; 9: 162-74.
[38] Erin N, Grahovac J, Brozovic A and Efferth T. Tumor microenvironment and epithelial mesenchymal transition as targets to overcome tumor multidrug resistance. Drug Resist Updat 2020; 53: 100715.
[39] Alban TJ, Alvarado AG, Sorensen MD, Bayik D, Volovetz J, Serbinowski E, Mulkearns-Hubert EE, Sinyuk M, Hale JS, Onzi GR, McGraw M, Huang P, Grabowski MM, Wathen CA, Ahluwalia MS, Radivoyevitch T, Kornblum HI, Kristensen BW, Vogelbaum MA and Lathia JD. Global immune fingerprinting in glioblastoma patient peripheral blood reveals immune-suppression signatures associated with prognosis. JCI Insight 2018; 3: e122264.
[40] Lin S, Zhang X, Huang G, Cheng L, Lv J, Zheng D, Lin S, Wang S, Wu Q, Long Y, Li B, Wei W, Liu P, Pei D, Li Y, Wen Z, Cui S, Li P, Sun X, Wu Y and Yao Y. Myeloid-derived suppressor cells promote lung cancer metastasis by CCL11 to activate ERK and AKT signaling and induce epithelial-mesenchymal transition in tumor cells. Oncogene 2021; 40: 1476-89.
[41] Wang L, Chang EW, Wong SC, Ong SM, Chong DQ and Ling KL. Increased myeloid-derived suppressor cells in gastric cancer correlate with cancer stage and plasma S100A8/A9 proinflammatory proteins. J Immunol 2013; 190: 794-804.
[42] Pardoll DM. The blockade of immune checkpoints in cancer immunotherapy. Nat Rev Cancer 2012; 12: 252-64.
[43] Picarda E, Ohaegbulam KC and Zang X. Molecular pathways: targeting B7-H3 (CD276) for human cancer immunotherapy. Clin Cancer Res 2016; 22: 3425-31.
[44] Kang R, Zhang Q, Zeh HJ 3rd, Lotze MT and Tang D. HMGB1 in cancer: good, bad, or both? Clin Cancer Res 2013; 19: 4046-57.
[45] Schoenfeld AJ and Hellmann MD. Acquired resistance to immune checkpoint inhibitors. Cancer Cell 2020; 37: 443-55.
[46] Weber R, Fleming V, Hu X, Nagibin V, Groth C, Altevogt P, Utikal J and Umansky V. Myeloid-derived suppressor cells hinder the anti-cancer activity of immune checkpoint inhibitors. Front Immunol 2018; 9: 1310.
[47] Hubert P, Roncarati P, Demoulin S, Pilard C, Ancion M, Reynders C, Lerho T, Bruyere D, Lebeau A, Radermecker C, Meunier M, Nokin MJ, Hendrick E, Peulen O, Delvenne P and Herfs M. Extracellular HMGB1 blockade inhibits tumor growth through profoundly remodeling immune microenvironment and enhances checkpoint inhibitor-based immunotherapy. J Immunother Cancer 2021; 9: e001966.
[48] Wang Y, Tong Z, Zhang W, Zhang W, Buzdin A, Mu X, Yan Q, Zhao X, Chang HH, Duhon M, Zhou X, Zhao G, Chen H and Li X. FDA-approved and emerging next generation predictive biomarkers for immune checkpoint inhibitors in cancer patients. Front Oncol 2021; 11: 683419.
[49] Orr B, Talje L, Liu Z, Kwok BH and Compton DA. Adaptive resistance to an inhibitor of chromosomal instability in human cancer cells. Cell Rep 2016; 17: 1755-63.
[50] Jost M, Chen Y, Gilbert LA, Horlbeck MA, Krenning L, Menchon G, Rai A, Cho MY, Stern JJ, Prota AE, Kampmann M, Akhmanova A, Steinmetz MO, Tanenbaum ME and Weissman JS. Pharmaceutical-grade rigosertib is a microtubule-destabilizing agent. Mol Cell 2020; 79: 191-8.
[51] Jost M, Chen Y, Gilbert LA, Horlbeck MA, Krenning L, Menchon G, Rai A, Cho MY, Stern JJ, Prota AE, Kampmann M, Akhmanova A, Steinmetz MO, Tanenbaum ME and Weissman JS. Combined CRISPRi/a-based chemical genetic screens reveal that rigosertib is a microtubule-destabilizing agent. Mol Cell 2017; 68: 210-23.

Table S1. TCGA study abbreviations

Study Abbreviation	Study name
LAML	Acute Myeloid Leukemia
ACC	Adrenocortical carcinoma
BLCA	Bladder Urothelial Carcinoma
LGG	Brain Lower Grade Glioma
BRCA	Breast invasive carcinoma
CESC	Cervical squamous cell carcinoma and endocervical adenocarcinoma
CHOL	Cholangiocarcinoma
COAD	Colon adenocarcinoma
ESCA	Esophageal carcinoma
GBM	Glioblastoma multiforme
HNSC	Head and Neck squamous cell carcinoma
KICH	Kidney Chromophobe
KIRC	Kidney renal clear cell carcinoma
KIRP	Kidney renal papillary cell carcinoma
LIHC	Liver hepatocellular carcinoma
LUAD	Lung adenocarcinoma
LUSC	Lung squamous cell carcinoma
DLBC	Lymphoid Neoplasm Diffuse Large B-cell Lymphoma
MESO	Mesothelioma
OV	Ovarian serous cystadenocarcinoma
PAAD	Pancreatic adenocarcinoma
PCPG	Pheochromocytoma and Paraganglioma
PRAD	Prostate adenocarcinoma
READ	Rectum adenocarcinoma
SARC	Sarcoma
SKCM	Skin Cutaneous Melanoma
STAD	Stomach adenocarcinoma
TGCT	Testicular Germ Cell Tumors
THYM	Thymoma
THCA	Thyroid carcinoma
UCS	Uterine Carcinosarcoma
UCEC	Uterine Corpus Endometrial Carcinoma
UVM	Uveal Melanoma

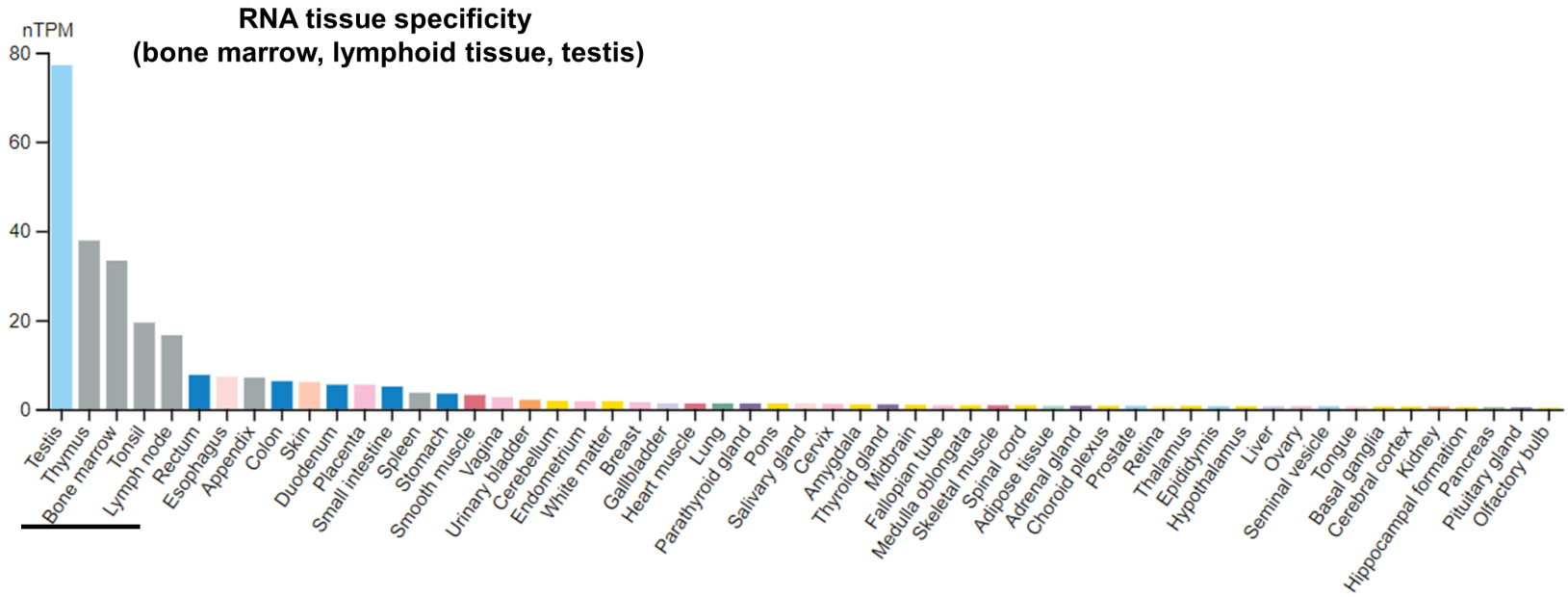

Figure S1. RNA expression level of *KIF2C* in different normal tissues using the consensus datasets of HPA and GTEx. nTPM, normalized transcripts per million.

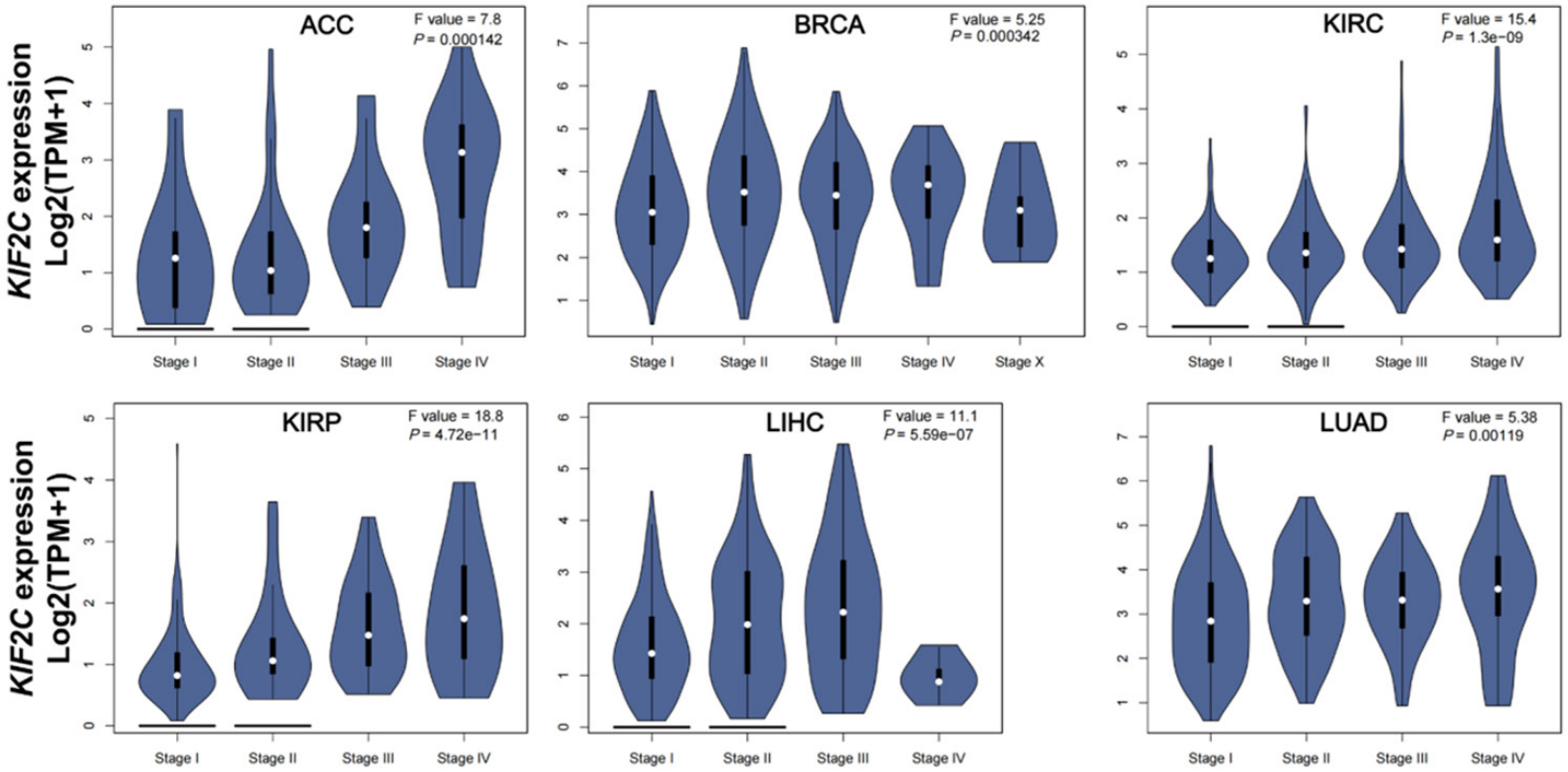

Figure S2. Expression status of *KIF2C* in various pathological stages of ACC, BRCA, KIRC, KIRP, LIHC, and LUAD in TCGA database. Log_2(TPM+1) transformed expression data for plotting, in one-way ANOVA. TPM, transcripts per million.

Table S2. RNA expression level of *KIF2C* in different cancer cell lines using the datasets of Cancer Cell Line Encyclopedia

Cancer cell line	n	Min	Max	Median	IQR	lower quartile	upper quartile	Mean	SD	SE
Bile Duct Cancer	35	2.379	6.229	4.878	1.186	4.248	5.434	4.756	0.940	0.159
Bladder Cancer	36	3.067	7.126	5.895	1.031	5.397	6.428	5.845	0.816	0.136
Bone Cancer	39	1.384	7.223	6.050	0.887	5.576	6.463	5.874	1.122	0.180
Brain Cancer	83	4.250	7.087	5.812	0.881	5.340	6.221	5.731	0.623	0.068
Breast Cancer	61	0.111	6.674	5.357	1.360	4.690	6.049	5.193	1.227	0.157
Cervical Cancer	17	2.809	6.949	5.733	0.873	5.078	5.950	5.391	0.972	0.236
Colon/Colorectal Cancer	71	3.002	6.377	5.298	0.760	4.807	5.567	5.154	0.619	0.073
Endometrial/Uterine Cancer	40	2.417	6.845	5.592	0.728	5.234	5.962	5.469	0.805	0.127
Other	14	4.103	6.843	5.092	0.986	4.672	5.658	5.212	0.786	0.210
Esophageal Cancer	32	2.698	6.367	5.436	0.855	4.972	5.827	5.335	0.738	0.130
Eye Cancer	11	2.287	6.392	4.983	1.831	3.636	5.467	4.455	1.356	0.409
Fibroblast	39	1.705	6.303	4.528	1.372	3.993	5.365	4.473	1.211	0.194
Gallbladder Cancer	6	4.487	5.911	4.955	0.487	4.657	5.144	5.012	0.515	0.210
Gastric Cancer	40	3.445	6.870	5.438	0.956	5.036	5.992	5.430	0.779	0.123
Head and Neck Cancer	56	1.050	6.688	5.188	0.934	4.746	5.680	5.036	1.098	0.147
Kidney Cancer	37	1.384	6.584	5.262	0.925	4.732	5.658	5.047	1.000	0.164
Leukemia	104	3.722	7.641	5.938	0.992	5.426	6.418	5.872	0.781	0.077
Liposarcoma	10	1.899	6.549	5.018	1.649	4.100	5.750	4.728	1.427	0.451
Liver Cancer	24	4.671	6.392	5.574	0.402	5.388	5.790	5.566	0.402	0.082
Lung Cancer	207	2.134	7.608	5.766	0.835	5.372	6.207	5.758	0.759	0.053
Lymphoma	83	2.834	7.092	5.914	0.868	5.335	6.203	5.638	0.854	0.094
Myeloma	30	2.524	6.953	5.399	1.200	4.685	5.884	5.247	0.958	0.175
Neuroblastoma	31	3.020	7.074	5.624	1.033	5.126	6.160	5.529	0.872	0.157
Ovarian Cancer	64	3.727	6.961	5.542	0.732	5.179	5.911	5.522	0.662	0.083
Pancreatic Cancer	52	3.141	6.461	5.304	0.881	4.870	5.751	5.223	0.764	0.106
Prostate Cancer	11	2.872	6.410	5.137	1.640	3.964	5.604	4.802	1.137	0.343
Rhabdoid	19	3.639	6.292	5.421	0.557	5.241	5.798	5.388	0.626	0.144
Sarcoma	36	3.406	6.812	5.984	0.821	5.515	6.336	5.853	0.726	0.121
Skin Cancer	85	2.104	6.657	5.447	0.900	4.941	5.841	5.323	0.807	0.088
Thyroid Cancer	17	3.438	6.811	5.757	1.321	5.070	6.391	5.619	0.967	0.235

Table S3. *KIF2C* correlated and interacted genes based on String, and GEPIA2

Correlated genes	Interacted genes
KIFC1	ADAM9
CDC20	ANAPC4
NCAPH	AURKA
KIF4A	BRCA1
DLGAP5	CCDC101
RAD54L	CENPH
CCNB2	CEP170
TPX2	CIT
CDCA5	DCTN1
CCNB1	DNAJA3
KIF20A	DNAJC16
NCAPG	DNAJC24
PLK1	DNM3
BUB1	ELAC2
CDCA8	ENSP00000351218
KIF23	ENSP00000423309
CENPA	GOT1
CCNA2	HIST1H4F
AURKB	HSPA14
KIF11	IRF2BP1
TTK	IRF2BP2
GTSE1	IRF2BPL
CDC25C	KIAA1429
NUSAP1	KIF14
CENPF	KIF18B
SKA1	KRT79
BIRC5	MAPRE1
HJURP	MAPRE2
NDC80	MAPRE3
ORC1	MTUS2
CCNF	NDEL1
AUNIP	NFYB
KIF15	NR2C2
CDCA3	PCBP2
PLK4	PLEKHA4
ASPM	PLK1
DEPDC1	POLR2J
PRC1	POLR2J2
EXO1	POLR2J3
TROAP	SGOL1
ZWINT	SGOL2
KIF18B	SKIV2L2
LMNB1	SMC4
NUF2	TEX10
CDK1	TUBA1A
RACGAP1	TUBB2B
SGOL1	UBE2A

KPNA2
CKAP2L
MCM6
UBE2C
MKI67
STIL
FOXM1
CHEK1
CENPI
SPC25
ESPL1
KIF14
KIF18A
NASP
GINS1
MAD2L1
UBE2T
MCM10
MCM2
TRAIP
FEN1
CEP55
FBXO5
EZH2
NEK2
LMNB2
CENPE
TIMELESS
CLSPN
CENPO
SGOL2
AURKA
RRM2
CDKN3
MTFR2
ORC6
CKS1B
KIAA1524
RAD51
FANCI
POC1A
C17orf53
CDC45
GSG2
PCNA
TUBB
TICRR
NDC1
ASF1B
MCM3

VHL
WDR5
WWP2

Table S4. Raw data of correlation of ImmuneScore, StromalScore, and ESTIMATEScore with *KIF2C* expression in tumors of TCGA database

Method	StromalScore	StromalScore	ImmuneScore	ImmuneScore	ESTIMATEScore	ESTIMATEScore
	pearson_R	pearson_P	pearson_R	pearson_P	pearson_R	pearson_P
TCGA-GBM (N=152)	-0.478015696	4.73E-10	-0.52299525	4.78E-12	-0.523088863	4.73E-12
TCGA-LGG (N=504)	0.17884494	5.40E-05	0.192550172	1.34E-05	0.192649711	1.33E-05
TCGA-UCEC (N=178)	-0.279938714	0.000154028	-0.23880383	0.001326574	-0.279230123	0.000160326
TCGA-BRCA (N=1077)	-0.271757112	1.09E-19	0.045661061	0.134255154	-0.107871407	0.000390636
TCGA-CESC (N=291)	-0.219102251	0.00016496	-0.218903033	0.000167295	-0.246136234	2.17E-05
TCGA-LUAD (N=500)	-0.195443152	1.07E-05	-0.203334744	4.58E-06	-0.21526221	1.18E-06
TCGA-ESCA (N=181)	-0.12909811	0.083262893	-0.230818843	0.001771052	-0.196104588	0.008150297
TCGA-SARC (N=258)	-0.212134752	0.000603664	-0.130038214	0.036847291	-0.173960939	0.005077828
TCGA-KIRP(N=285)	0.029323353	0.622036895	-0.06709912	0.258873328	-0.030520905	0.607876274
TCGA-COAD (N=282)	-0.177838376	0.00272583	-0.034427241	0.564794652	-0.116816156	0.050033446
TCGA-PRAD (N=495)	0.053609608	0.233818785	0.128081314	0.004314685	0.103221195	0.02162683
TCGA-STAD (N=388)	-0.441957732	5.53E-20	-0.286007946	9.71E-09	-0.39661363	4.56E-16
TCGA-HNSC (N=517)	-0.219455554	4.67E-07	-0.044501316	0.312540412	-0.143287341	0.001086928
TCGA-KIRC (N=528)	0.140977402	0.001162308	0.283183727	3.41E-11	0.249770934	5.95E-09
TCGA-LUSC (N=491)	-0.336871055	1.71E-14	-0.313994352	1.07E-12	-0.344150832	4.25E-15
TCGA-THYM (N=118)	-0.309581259	0.000646491	0.397472834	8.32E-06	0.134604375	0.146158541
TCGA-LIHC (N=363)	-0.193379029	0.000209973	0.099097979	0.059267557	-0.027629768	0.599790125
TCGA-SKCM (N=452)	-0.16709726	0.000359971	-0.129790224	0.005719648	-0.154185568	0.001006729
TCGA-BLCA (N=405)	-0.048955916	0.325724072	-0.014378198	0.772982234	-0.033714882	0.498663483
TCGA-THCA (N=503)	0.142068725	0.001400442	0.154238358	0.000517764	0.160025473	0.000314184
TCGA-MESO (N=85)	0.113945749	0.299102554	0.053366187	0.627624621	0.090102175	0.412175507
TCGA-READ (N=91)	-0.176914694	0.093427301	-0.165060017	0.117923078	-0.181256115	0.085533544
TCGA-OV (N=417)	-0.150964292	0.001993097	-0.062952363	0.199513936	-0.112556056	0.021512329
TCGA-UVM (N=79)	0.118952945	0.296421805	0.200700349	0.076141976	0.18428318	0.103993424
TCGA-PAAD (N=177)	-0.045709731	0.54575349	-0.013690528	0.85647856	-0.031022353	0.681879306
TCGA-TGCT (N=132)	-0.341744567	6.06E-05	-0.297988704	0.000519973	-0.383328845	5.71E-06
TCGA-UCS (N=56)	-0.131474742	0.334105463	-0.319814766	0.016271282	-0.263921321	0.0493607
TCGA-LAML (N=214)	0.36503155	3.81E-08	-0.043725554	0.524641027	0.148862723	0.02947578
TCGA-PCPG (N=177)	0.121051911	0.108496425	-0.04859084	0.520705471	0.039691796	0.599909732
TCGA-ACC (N=77)	-0.08559381	0.459204414	-0.143133613	0.214290192	-0.124105312	0.282208595
TCGA-DLBC (N=46)	0.077241455	0.609895224	-0.217685552	0.146147029	-0.091145102	0.546894819
TCGA-KICH (N=65)	0.099031024	0.432539226	-0.028109985	0.824098662	0.028336194	0.822706015
TCGA-CHOL (N=36)	-0.26448767	0.119037384	-0.078328286	0.649769493	-0.156805468	0.361086544